TUM/T39-98-3
UG-DFM-10/97

Double$-\Lambda$ Hypernuclei and the Nuclear Medium Effective $\Lambda\Lambda$ Interaction.

José Caro[1], Carmen García-Recio[2] and Juan Nieves[2]

[1] Physik Department, Technische Universität-München, D-85747-Garching, Germany.
[2] Departamento de Física Moderna, Universidad de Granada, E-18071 Granada, Spain.

Abstract

We fit the ${}^1S_0$ $\Lambda\Lambda$ interaction in the nuclear medium to the masses of the experimentally known double$-\Lambda$ hypernuclei: ${}^{\ 6}_{\Lambda\Lambda}$He, ${}^{10}_{\Lambda\Lambda}$Be and ${}^{13}_{\Lambda\Lambda}$B. We derive this effective interaction from OBE Jülich $\Lambda\Lambda$-type potentials and using both Hartree-Fock and variational approaches. We find that the inclusion of $\Lambda\Lambda$ correlations in the variational scheme leads to significant differences and a better understanding of the dynamical features of the system. We investigate the sensitivity of the binding energies and the mesonic decay widths of the above double$-\Lambda$ hypernuclei to the $\omega\Lambda\Lambda$ coupling and the form factor at the $\sigma\Lambda\Lambda$ vertex. We also use this effective interaction to predict binding energies and pionic decay widths of heavier double$-\Lambda$ hypernuclei, not discovered yet. Finally, we discard the existence of ${}^1S_0$ $\Lambda\Lambda$ bound states provided the $\Lambda\Lambda - \Xi N$ coupling can be neglected.

PACS: 21.80.+a,21.30.-x,21.10.Dr,21.45+v
Keywords: single and double$-\Lambda$ hypernuclei, $\Lambda\Lambda$ interaction, Bonn potential, Jülich potential, effective interactions, two-body correlations, mesonic decay.

Hypernucleus	$B_{\Lambda\Lambda}$(MeV)	$\Delta B_{\Lambda\Lambda}$(MeV)
${}^{6}_{\Lambda\Lambda}$He [5], [10]	10.9 ± 0.8	4.7 ± 1.0
${}^{10}_{\Lambda\Lambda}$Be [6], [10]	17.7 ± 0.4	4.3 ± 0.4
${}^{13}_{\Lambda\Lambda}$B [7], [10]	27.5 ± 0.7	4.8 ± 0.7

Table 1: Experimental double$-\Lambda$ hypernuclei binding energies, $B_{\Lambda\Lambda}$, and values for the quantity $\Delta B_{\Lambda\Lambda}$ defined in Eq. (2). As it is discussed with great detail in [25], we have considered that the event reported by [7] corresponds to the double$-\Lambda$ hypernucleus ${}^{13}_{\Lambda\Lambda}$B. We use the notation ${}^{A+2}_{\Lambda\Lambda}Z$.

1 Introduction

In the past years a considerable amount of work has been done both in the experimental ([1]-[11]) and the theoretical ([12]-[41]) aspects of the physics of single and double$-\Lambda$ hypernuclei (for a general overview see the proceedings of the most recent *International Conferences on Hypernuclear and Strange Particle Physics* [42]).

Up to now, the experimental community has reported the existence and has measured the ${}^1S_0$ ground state (angular momentum and spin of the two interacting Λ's coupled to zero, $L = S = 0$) binding energy of three double$-\Lambda$ hypernuclei[1]: ${}^{6}_{\Lambda\Lambda}$He, ${}^{10}_{\Lambda\Lambda}$Be and ${}^{13}_{\Lambda\Lambda}$B which energies are reported in Table 1. Let us consider the hypernucleus ${}^{A+2}_{\Lambda\Lambda}Z$, composed of a nuclear core ${}^{A}Z$ and two bound Λ particles. The quantity $B_{\Lambda\Lambda}$ is defined as the total binding energy (> 0) of the double$-\Lambda$ hypernucleus, and thus it is given by

$$B_{\Lambda\Lambda} \;=\; -\left[M\left({}^{A+2}_{\Lambda\Lambda}Z\right) - M\left({}^{A}Z\right) - 2m_{\Lambda}\right], \tag{1}$$

where $M(\cdots)$ denotes the mass of the system which appears inside the brackets and m_Λ (1115.6 MeV) is the Λ mass. To learn about the nature of the $\Lambda\Lambda$ interaction, it is usual to define the magnitude $\Delta B_{\Lambda\Lambda}$ as

$$\Delta B_{\Lambda\Lambda} \;=\; B_{\Lambda\Lambda} - 2B_{\Lambda}, \tag{2}$$

where B_Λ (> 0), given by

$$B_{\Lambda} \;=\; -\left[M\left({}^{A+1}_{\Lambda}Z\right) - M\left({}^{A}Z\right) - m_{\Lambda}\right], \tag{3}$$

is the binding energy of a hyperon Λ in the hypernucleus ${}^{A+1}_{\Lambda}Z$. Neglecting saturation effects, $\Delta B_{\Lambda\Lambda}$ is suppressed with respect to $B_{\Lambda\Lambda}$ by one power of the nuclear mass number.

Data on Λ-proton scattering constitute an indirect source of information about the $\Lambda\Lambda$ interaction. Although the available hyperon-nucleon scattering data are scarce, this

[1]There has been some confusion about the exact nature of the event reported by Aoki. et. al. [7]. This event was identified as ${}^{10}_{\Lambda\Lambda}$Be or ${}^{13}_{\Lambda\Lambda}$B, resulting, respectively, in a repulsive or attractive $\Lambda\Lambda$ interaction. However, the theoretical analysis of Yamamoto et. al. [24] and Dover et. al. [25] helped to discard the possibility of ${}^{10}_{\Lambda\Lambda}$Be, and thus it is commonly accepted an attractive nature for the $\Lambda\Lambda$ interaction.

information has been successfully used by the Nijmegen [43, 44], Jülich [45, 46] and Tübingen [47, 48] groups to determine realistic hyperon-nucleon and thus also some pieces of the hyperon-hyperon interactions. The Tübingen model is mainly a constituent quark model supplemented in the long and intermediate range part by π and σ exchange; the latter is treated as an $SU(3)$ singlet, with a mass of 520 MeV. On the other hand, the Nijmegen and Jülich models are based on meson exchange. In both models most of the required intermediate range attraction is provided by the exchange of mesons in the scalar-isoscalar channel.

The Jülich YN interaction models have been constructed following the same ideas as those used in the Bonn NN potential [49]. Thus, these models account for the intermediate range attraction by the exchange of a fictitious scalar-isoscalar meson, σ, with a mass of about 600 MeV. The σ is not treated as a physical particle to which the $SU(3)$ relations should be applied, but merely as an effective description of correlated 2π and $K\bar{K}$-exchange processes. However, the Nijmegen group views the scalar-isoscalar interaction as generated by genuine scalar meson exchanges (S^*, δ, ϵ and κ). Then, the $SU(3)$ symmetry is used to relate the couplings of the above mesons to the nucleons and hyperons.

Jülich and Nijmegen models, or some inspired in them, have been extensively used to analyze single–Λ hypernuclei [15, 17, 21, 31, 33, 36].

Because the direct measurement of the $\Lambda\Lambda$ scattering process is impractical due to the lack of targets, the data on $\Lambda\Lambda$ hypernuclei provide a unique method to learn details on the $\Lambda\Lambda$ interaction in the vacuum. Thus, since the first double$-\Lambda$ hypernuclei were discovered, suggestions to extract the vacuum $\Lambda\Lambda$ interaction from these systems were made [50]. Since then, many other authors have tried to shed light on this interesting issue [16, 18, 24, 27, 28, 35, 37]. Near threshold $(2m_\Lambda)$, the S (strangeness) $= -2$ baryon-baryon interaction might be described in terms of only two couple channels [24]: $\Lambda\Lambda$ and ΞN. For two Λ hyperons bound in a nuclear medium and because of Pauli-blocking, it is reasonable to think that the ratio of strengths of the $\Lambda\Lambda \to \Xi N \to \Lambda\Lambda$ and the diagonal $\Lambda\Lambda \to \Lambda\Lambda$ (with no ΞN intermediate states) transitions is suppressed respect to the free space case. This is explicitly shown for ${}^{\;\;6}_{\Lambda\Lambda}$He in Ref. [37]. Thus, the data of double$-\Lambda$ hypernuclei would mainly probe the free space diagonal $\Lambda\Lambda$ element of the $\Lambda\Lambda - \Xi N$ potential. In principle, some information about this piece can be extracted from the hyperon-nucleon interaction models developed by the Nijmegen, Jülich and Tübingen groups.

In references [16, 18] a variational approach and a α-cluster decomposition of the considered nuclear cores (^{4}He and ^{8}Be) are used. However, neither the Nijmegen nor the Jülich or Tübingen models for the $\Lambda\Lambda$ interaction are used in these references. In Refs. [24, 27, 28, 37] different Nijmegen $\Lambda\Lambda$ interactions are considered and $G-$matrix calculations show that the double$-\Lambda$ hypernuclei data favor the Nijmegen model D. Despite of the success of Jülich type ΛN interactions to describe the structure of single–Λ hypernuclei physics [21, 33, 36], double$-\Lambda$ hypernuclei studies using Jülich $\Lambda\Lambda$ one boson exchange (OBE) potentials have not been performed yet.

Other problems of great interest connected with the $\Lambda\Lambda$ hypernuclear physics are the possible existence of the $S = -2$ six quark H dibaryon [51, 52], and the breaking of $SU(3)$ symmetry in baryon-baryon interactions [53]. Six quarks bound states would explore new dynamical features of the color interactions different to those accessible by means of the study of *normal* mesons ($q\bar{q}$) and baryons (qqq). The existence of $\Lambda\Lambda$ bound states may obstruct the experimental detection of the dibaryon H. On the other hand, some authors have shown that the existence of double$-\Lambda$ hypernuclei restricts the feasibility of a long-living H dibaryon [54].

The experimental community has also invested a lot of effort in the subject, partially aimed to discover the H particle (see Refs. [8]-[10]). Both at KEK and at BNL facilities, cascade particles (Ξ^-) are being produced by means of the (K^-, K^+) reaction and then stopped in matter to produce $S = -2$ nuclei. At KEK it is planned [9] to increase the number of stopped Ξ^- events by roughly a factor 10 with respect to the experience of Refs. [7, 8], where the double$-\Lambda$ hypernuclei ${}^{13}_{\Lambda\Lambda}$B was first discovered. At BNL the reaction

$$\Xi^- \, {}^{A}Z \;\; \rightarrow \;\; {}^{A}_{\Lambda\Lambda}(Z-1) \;\; n, \tag{4}$$

will be used to produce light and medium double$-\Lambda$ hypernuclei [10, 11].

This work is the first of a series of two where we aim to describe the $\Lambda\Lambda$ interaction, both inside of the nuclear medium and in the vacuum. In this first work we find the effective $\Lambda\Lambda$ potential in the medium. Elsewhere we study the nuclear medium modifications of the $\Lambda\Lambda$ interaction and from this study and the effective potential obtained here we will try to extract the $\Lambda\Lambda$ interaction in the free space, including its spin dependence [55].

In this paper, we take the Jülich model for the interaction between the two Λ hyperons and fit its parameters to the binding energies of the three experimentally known double$-\Lambda$ hypernuclei. This model does not account for ΞN intermediate states. Thus, the $\Lambda\Lambda$ diagonal interaction parameters fitted here, might effectively include some contributions from this non-elastic intermediate channel, though we expect them to be reasonably small, as discussed above. We use three different approaches: perturbative, Hartree-Fock and variational, and find that, though the first two are practically equivalent, the inclusion of $\Lambda\Lambda$ correlations in the variational scheme leads to significant differences and a better understanding of the dynamical features of the system. We also study the sensitivity of the hypernuclear data to the cutoff masses, used in the Jülich model for the $\Lambda\Lambda$ interaction, and also examine potentials with dynamical breaking of the $SU(3)$ symmetry. Thus, we end up with a whole family of potentials describing the ground state binding energy of the three known double$-\Lambda$ hypernuclei. With the aim of trying to distinguish between the different potentials, we calculate the mesonic decay width of boron double$-\Lambda$ hypernuclei. Finally, we predict binding energies and mesonic widths of heavier hypernuclei, not detected yet, we discuss the possible existence of $\Lambda\Lambda$ bound states and devote a few words to relate the free space $\Lambda\Lambda$ interaction to that found in this work.

The paper is organized as follows. Our approach to the double$-\Lambda$ hypernuclei is described in Sect. 2, including the details on the $\Lambda\Lambda$ interaction. In Sect. 3 our model to

the mesonic decay of double−Λ hypernuclei is discussed. Results are presented in Sect. 4, which is split in different subsections: *"Λ-core potentials"*, *"ΛΛ interaction: Hartree-Fock results"*, *"Perturbative approach"*, *"ΛΛ interaction: variational results"*, *"Contribution of the $\phi-$exchange"* , *"Mesonic decay and binding energies of double−Λ hypernuclei"* and *"Nuclear medium and free space ΛΛ interactions."* Finally in Sect. 5 we present our conclusions. In addition, there is an appendix, where we give some of the needed matrix elements within the variational scheme.

2 Model for the Double−Λ Hypernuclei

We approximate the double−Λ hypernuclei by systems composed by two interacting Λ's moving in the mean field potential created by the nuclear cores ($\mathcal{V}_{\Lambda A}$). Thus, we solve

$$\left[\sum_{i=1,2}\left(-\frac{\vec{\nabla}_i^2}{2\mu_A}+\mathcal{V}_{\Lambda A}(\vec{r_i})\right)+V_{\Lambda\Lambda}(\vec{r_1}-\vec{r_2})-\frac{\vec{\nabla}_1\cdot\vec{\nabla}_2}{M_A}+B_{\Lambda\Lambda}\right]\mathbf{\Phi_{\Lambda\Lambda}}(\vec{r_1},\vec{r_2}) \;=\; 0, \quad (5)$$

where M_A and μ_A are the nuclear core and the Λ-core reduced masses respectively, $\mathbf{\Phi_{\Lambda\Lambda}}(\vec{r_1},\vec{r_2})$ is the wave–function of the ΛΛ pair and the $\vec{\nabla}_1\cdot\vec{\nabla}_2$ piece is the Hughes-Eckart (HE) term [56]. The spin dependence in the equation above is implicit in the operators and wave–function. The Λ-nuclear core potential, $\mathcal{V}_{\Lambda A}$, is adjusted to reproduce the binding energies of the corresponding single–Λ hypernuclei and a σ-ω meson exchange potential is used for the ΛΛ interaction in the medium, $V_{\Lambda\Lambda}$. More details will be given in the next subsections.

In this approximation we neglect the dynamical re-ordering effect in the nuclear core due to the presence of the second Λ and assume that both hyperons move in the same mean field as one single hyperon does. Both, the ΛΛ interaction and this re-ordering of the nuclear core, contribute to $\Delta B_{\Lambda\Lambda}$. However, the latter effect is suppressed with respect to the former by one power of the nuclear density, which is the natural parameter in all many body quantum theory expansions [57]. Thus, we expect the nuclear core dynamical re-ordering effects to be of the order of $\Delta B_{\Lambda\Lambda}/A$, that is to say around 0.5 MeV for beryllium and boron and around 1 MeV for helium. However, in view of the large binding and incompressibility of an α particle, it is reasonable to think that the nuclear-core distortion effects in helium will not be as large as the naive estimate given above. Thus, we will assume an uncertainty of the order of 0.5 MeV in all hypernuclei due to these effects, which is of the order of the experimental errors of $B_{\Lambda\Lambda}$ reported in Table 1. This lack of our model will be translated into an increase of the size of the systematic error of our determination of the ΛΛ potential in the medium.

To take properly into account, in the boron region, the effects due to dynamical re-ordering in the nuclear core is out of the scope of this paper. Indeed, it would likely require the use of variational montecarlo techniques to solve the system of $A+2$ interacting particles and the use of realistic NN, ΛN and ΛΛ interactions. The only attempt to take partially into account these effects can be found in Refs. [16, 18, 50] for the case of

${}^{10}_{\Lambda\Lambda}$Be. There, the ^{8}Be nuclear core is described in terms of two interacting α particles and the corresponding four-body ($\alpha\alpha\Lambda\Lambda$) problem is solved and it is found that nuclear core polarization effects change $B_{\Lambda\Lambda}$ by about 0.5 MeV, in agreement with our previous estimate based in qualitative arguments. This model, however, is difficult to use for any other nuclear core that beryllium.

Note also that the HE term, which naturally appears in our framework, contributes to $\Delta B_{\Lambda\Lambda}$ and accounts for the variation of the core–kinetic energy due to the presence of the second Λ. As we will see, this piece improves the simultaneous description of an extremely light hypernucleus, as helium, and not as light ones, as beryllium or boron.

Taking into account Fermi statistics for the system of two identical Λ's, the most general wave function in the $^1S_0$ channel is given by

$$\mathbf{\Phi_{\Lambda\Lambda}}(\vec{r_1},\vec{r_2}) \;=\; K\left[f(r_1,r_2,r_{12})+f(r_2,r_1,r_{12})\right]\;\chi^{S=0}, \tag{6}$$

where K is a normalization constant, $r_{12}=|\vec{r_1}-\vec{r_2}|$ and $\chi^{S=0}$ represents the spin-singlet.

It is also interesting to define the density of probability, $\mathbf{P}(r_{12})$, of finding the two Λ particles at relative distance r_{12}. This is given by

$$\mathbf{P}(r_{12}) \;=\; \int d^3r_1 \int d^3r_2\, \delta\left(|\vec{r_1}-\vec{r_2}|-r_{12}\right) \left|\mathbf{\Phi_{\Lambda\Lambda}}(\vec{r_1},\vec{r_2})\right|^2 . \tag{7}$$

We apply both the Hartree-Fock (HF) and variational (VAR) approximations to solve Eq. (5).

In the HF approach, the wave function of the two Λ's is given by

$$\mathbf{\Phi^{HF}_{\Lambda\Lambda}}(\vec{r_1},\vec{r_2}) \;=\; \phi_\Lambda(\vec{r_1})\;\phi_\Lambda(\vec{r_2})\;\chi^{S=0}, \tag{8}$$

$$\phi_\Lambda(\vec{r}) \;=\; R_\Lambda(r)\;Y_{00}(\hat{r}), \tag{9}$$

where $Y_{lm}(\hat{r})$ are the spherical harmonics and $R_\Lambda(r)$ represents the mono-particle radial wave function which is obtained using a self-consistent procedure [56].

In the VAR approach we allow for a wider family of wave–functions $\mathbf{\Phi_{\Lambda\Lambda}}(\vec{r_1},\vec{r_2})$, including $r_{12}-$correlations. In analogy with calculations on the atomic three–body problem [58] – [61], we use a series of standard Hylleraas type wave functions [62] to expand the wave–function of the two Λ's system. Thus, our ansatz for the wave function is

$$\mathbf{\Phi^{VAR}_{\Lambda\Lambda}}(\vec{r_1},\vec{r_2}) \;=\; \left[\sum_{abc}^{\infty} C_{abc}(r_1^a r_2^b + r_1^b r_2^a)\, r_{12}^c \exp\left\{-\alpha(r_1+r_2)\right\}\right]\;\chi^{S=0}, \tag{10}$$

with α a real parameter, a,b,c non–negative integer numbers and $a\leq b$. Note that, even in the case $c=0$, where no correlations of the type r_{12} are included, this variational scheme does not reduce to the HF one because our ansatz of Eq. (10) can not be always gathered as the product of a function which depends only on the radial coordinate r_1 times the same function of the radial coordinate r_2. We would like to mention that, though

the expected value of the HE term is zero in the HF ground state, it is not when VAR wave–functions, with explicit dependence on r_{12}, are used.

For practical purposes, the latter series should be truncated and following the findings in atomic physics [59] we choose to fix

$$a + b + c \leq N, \tag{11}$$

Thus, the integer number N determines the dimension, $N_{\rm EL}$, of our basis[2]. The unknown parameters, α and C_{abc}, are to be determined to give the lowest value of the energy. The linear parameters C_{abc} are obtained by solving a generalized eigenvalue problem [63], while to find the non-linear parameter α one needs to use a standard numerical minimization algorithm. We have performed calculations up to $N = 10$ for which we estimate that the uncertainties in the determination of the binding energies, $B_{\Lambda\Lambda}$, are one order of magnitude smaller than their experimental errors. Our ansatz for $\mathbf{\Phi}^{\mathbf{VAR}}_{\mathbf{\Lambda\Lambda}}$ and $N = 10$ consists of 161 terms. In atomic physics with such a basis one gets precisions of the order of 10^{-6}, [60, 61], much better than those obtained here. That is because the ratio between the mass of the orbiting particles and the mass of the nuclear core is much more bigger here than in the case of two electrons bound systems. The accuracy could be improved by allowing for different exponential behaviors for the radial coordinates r_1 and r_2 and symmetrizing the resulting wave function [64].

In the VAR approach, each of the Λ particles is orbiting around the nuclear core not only in the l=0 wave, as in the HF case. Indeed, if the angular momenta of the two Λ's are coupled to give zero total angular momentum ($\vec{L} = \vec{l_1} + \vec{l_2} = \vec{0}$), any Λ-nuclear core orbital angular momentum is permitted. Of course, the only possibility is that both Λ's have the same orbital angular momentum, $l_1 = l_2 = l$, with respect to the nuclear core.

Given a wave function for the two Λ's system $\mathbf{\Phi_{\Lambda\Lambda}}(r_1, r_2, r_{12})$, the probability, $\mathcal{P}_l$, of finding each of the two particles with angular momentum l and coupled to $L = 0$ is given by

$$\mathcal{P}_l \;=\; 4\pi^2(2l+1)\int_0^{+\infty} dr_1\; r_1^2 \int_0^{+\infty} dr_2\; r_2^2 \left|\int_{-1}^{+1} d\mu\; P_l(\mu)\mathbf{\Phi_{\Lambda\Lambda}}(r_1, r_2, r_{12})\right|^2, \tag{12}$$

where P_l is the Legendre Polynomial of order l and μ is the cosine of the angle between the vectors $\vec{r}_1$ and $\vec{r}_2$, being $r_{12} = (\, r_1^2 + r_2^2 - 2r_1r_2\mu)^{\frac{1}{2}}$.

In Refs. [16] and [18], the problem of double$-\Lambda$ hypernuclei using a variational approach was also addressed. However, the configuration space for the trial wave function ($\mathbf{\Phi}^{\mathbf{VAR}}_{\mathbf{\Lambda\Lambda}}$), used in these references to describe the $\Lambda\Lambda$ relative motion, is much more reduced than the one used in this work.

[2] $N_{\rm EL}$ is given by

$$N_{\rm EL} = \begin{cases} \frac{1}{24}(2N^3 + 15N^2 + 34N + 24) & N \text{ even} \\ \\ \frac{1}{24}(2N^3 + 15N^2 + 34N + 21) & N \text{ odd} \end{cases}$$

With a basis of the size of the one used here, one needs to compute more than twenty five thousand matrix elements of the Hamiltonian, for each value of α. Furthermore, because of the non-orthogonality of the chosen basis there exist large numerical cancelations in the linear parameters (C_{abc}) minimization process and it is necessary to have analytical expressions for the matrix elements. These can be found in the Appendix.

2.1 Model for the $\Lambda\Lambda$ Interaction

Given the quantum numbers of the Λ particle, the lightest carriers of the strong interaction between two Λ's, in the scalar-isoscalar and vector-isoscalar channels, are the $\sigma\,(I = 0,\, J^P = 0^+)$ and $\omega\,(I = 0,\, J^P = 1^-)$ mesons, respectively. As it was mentioned in the introduction, the σ is not treated as a physical particle, but merely as an effective description of correlated 2π and $K\bar{K}$-exchange processes, as it is done in the context of the Jülich models for YN interaction [45, 46]. The η and η' meson exchanges lead to a $\Lambda\Lambda$ potentials in the pseudoscalar-isoscalar channel which contributions are negligible at low momentum transfers [3], and are not considered in the context of the Jülich models for YN interaction [45, 46]. Thus, we will not consider those in this work.

In the spirit of the Bonn-Jülich potentials, we should also study the exchange of the $\phi\,(I = 0,\, J^P = 1^-)$ meson. In Ref. [35], where the Nijmegen model D contributions of different mesons are studied and compared for the $^1S_0$ $\Lambda\Lambda$ system, it is shown that the contribution next in importance to that of the σ and ω mesons is the $\phi-$ exchange, being its contribution attractive. By taking the so-called "ideal" mixing angle ($\tan\theta_v = 1/\sqrt{2}$), the ϕ meson comes out as a pure $s\bar{s}$ state and thus in Refs. [45, 46] a vanishing ϕNN coupling is required. This provides a relation between the singlet and octet couplings, which determines the $\phi\Lambda\Lambda$ couplings in terms of the $\omega\Lambda\Lambda$ ones.

The mass of the ϕ meson is significantly larger ($m_\phi = 1019.41$ MeV) than those of the σ and ω mesons. Then its contribution will be relevant at very short distances, where any potential model based on meson exchanges suffers of some uncertainties which are translated into the inclusion of form-factors and uncertainties in the precise values and shapes of them. To explore the dynamics at short distances one needs high momentum transfers, thus though one might expect the $\phi-$exchange to be relevant in scattering processes at large energies and scattering angles, it is also reasonable to think that such contribution is much less relevant to study the dynamics of a $\Lambda\Lambda$ pair below threshold. Furthermore, because the ϕ meson does not couple to nucleons within the Bonn-Jülich model, its contribution was not taken into account in their phenomenological studies of the NN and YN scattering data. Thus, we count with any empirical determination neither of the ϕNN nor of the $\phi\Lambda\Lambda$ form-factors. We have checked that the importance of the $\phi-$exchange in the $^1S_0$ $\Lambda\Lambda$ system at threshold is small and, depends strongly on the used form-factor, as one could expect. Taking as reference the cutoff used for the $\omega-$exchange, we find that small changes in the cutoff lead to big changes in the small role played by the ϕ meson in double$-\Lambda$ hypernuclei. Given that we count with only three piece of data, that

[3] This is explicitly shown in Refs. [35, 44] also for the Nijmegen model D.

we expect the $\phi-$ exchange contribution to be small and furthermore is not completely determined by that of the $\omega-$ exchange and thus its inclusion would require additional free parameters, we will not include the $\phi-$ exchange from the beginning. We will try to keep our model for the effective $\Lambda\Lambda$ interaction in the medium reasonably simple, and thus we will construct it in terms only of $\sigma-$ and $\omega-$exchanges. In any case, in Subsect. 4.5 we will discuss qualitatively and quantitatively the influence of the $\phi-$exchange in the results presented through the paper.

Apart from single meson exchanges, in principle, one should also include the $\Lambda\Lambda - \Xi N$ coupling, as mentioned in the Introduction. For simplicity, we will first ignore this possibility. The possible contribution of this coupled channel and that of the ϕ meson exchange (and that of heavier mesons, not explicitly mentioned in this discussion) will be in any case accounted for in the obtained effective coupling constants of the considered σ and ω exchanges. We will comment on this when we try to link the effective $\Lambda\Lambda$ interaction obtained in this work, from the double$-\Lambda$ hypernuclei data, to the interaction in the free space.

The couplings of the σ and ω mesons to the Λ are described by the following interaction Lagrangians [36, 45]:

$$\mathcal{L}_{\sigma\Lambda\Lambda} = g_{\sigma\Lambda\Lambda}\bar{\Psi}_\Lambda(x)\phi_\sigma(x)\Psi_\Lambda(x), \tag{13}$$

$$\mathcal{L}_{\omega\Lambda\Lambda} = g_{\omega\Lambda\Lambda}\bar{\Psi}_\Lambda(x)\gamma_\mu\phi^\mu_\omega(x)\Psi_\Lambda(x) + \frac{f_{\omega\Lambda\Lambda}}{4m_N}\bar{\Psi}_\Lambda(x)\sigma_{\mu\nu}\Psi_\Lambda(x)\left(\partial^\mu\phi^\nu_\omega(x) - \partial^\nu\phi^\mu_\omega(x)\right) \tag{14}$$

where we have used $m_N = 938.926\,\mathrm{MeV}$ for the nucleon mass. Ψ_Λ, ϕ_σ and ϕ_ω are the Λ, σ and ω fields, γ^μ are the Dirac matrices and $\sigma^{\mu\nu} = i[\gamma^\mu, \gamma^\nu]/2$. The parameter $f_{\omega\Lambda\Lambda}$ accounts for the tensorial part of the $\omega\Lambda\Lambda$ coupling.

The $\Lambda\Lambda$ OBE potential in configuration space is obtained via Fourier transform from the $\Lambda\Lambda$ Feynman amplitudes[4] obtained from the above Lagrangians and reads [49]

$$\begin{aligned}
V_\sigma(m_\sigma, r) &= -\frac{g^2_{\sigma\Lambda\Lambda}}{4\pi}m_\sigma\left\{\left[1 - \frac{1}{4}\left(\frac{m_\sigma}{m_\Lambda}\right)^2\right]Y(m_\sigma r)\right. \\
&+ \left.\frac{1}{4m^2_\Lambda}\left[\nabla^2 Y(m_\sigma r) + Y(m_\sigma r)\nabla^2\right] + \frac{1}{2}Z_1(m_\sigma r)\vec{L}\cdot\vec{S}\right\}, \qquad (15)\\
V_\omega(m_\omega, r) &= \frac{g^2_{\omega\Lambda\Lambda}}{4\pi}m_\omega\left\{\left[1 + \frac{1}{2}\left(\frac{m_\omega}{m_\Lambda}\right)^2\right]Y(m_\omega r) - \frac{3}{4m^2_\Lambda}\left[\nabla^2 Y(m_\omega r) + Y(m_\omega r)\nabla^2\right]\right. \\
&+ \left.\frac{1}{6}\left(\frac{m_\omega}{m_\Lambda}\right)^2 Y(m_\omega r)\,\vec{\sigma_1}\cdot\vec{\sigma_2} - \frac{3}{2}Z_1(m_\omega r)\vec{L}\cdot\vec{S} - \frac{1}{12}Z(m_\omega r)S_{12}\right\} + \\
&+ \frac{1}{2}\frac{g_{\omega\Lambda\Lambda}f_{\omega\Lambda\Lambda}}{4\pi}m_\omega\frac{m_\Lambda}{m_N}\left\{\left(\frac{m_\omega}{m_\Lambda}\right)^2 Y(m_\omega r) + \frac{2}{3}\left(\frac{m_\omega}{m_\Lambda}\right)^2 Y(m_\omega r)\,\vec{\sigma_1}\cdot\vec{\sigma_2}\right.
\end{aligned}$$

[4] A non-relativistic expansion of the amplitudes is performed, keeping only up to quadratic terms in momenta over baryon masses.

$$
\begin{aligned}
&- \quad 4Z_1(m_\omega r)\vec{L}\cdot\vec{S} - \frac{1}{3}Z(m_\omega r)S_{12}\Big\} \\
&+ \quad \frac{f^2_{\omega\Lambda\Lambda}}{4\pi}\left(\frac{m_\Lambda}{m_N}\right)^2 m_\omega \left\{\frac{1}{6}\left(\frac{m_\omega}{m_\Lambda}\right)^2 Y(m_\omega r)\,\vec{\sigma_1}\cdot\vec{\sigma_2} - \frac{1}{12}Z(m_\omega r)S_{12}\right\}, \qquad (16)
\end{aligned}
$$

$$
Y(x) = \frac{e^{-x}}{x}, \quad \nabla^2 = \frac{1}{r}\frac{d^2}{dr^2}r - \frac{\vec{L}^{\,2}}{r^2}, \qquad (17)
$$

where $m_{\sigma\,(\omega)}$ is the $\sigma\,(\omega)$ meson mass for which we take 550 (782.6) MeV. The operators $\vec{\sigma}$, $\vec{S}$, $\vec{L}$ and S_{12} are the Pauli matrices, total spin and angular momentum and the second order rank spin tensor operator respectively. Finally, the functions Z, Z_1 can be found in [49].

The potentials should also contain form factors describing the extended hadron structure. Although they in general depend on all the three four-momenta involved at the vertex, they are usually parameterized in a simple form depending only on the four-momentum, q, of the exchanged meson. Taking a monopolar form and neglecting the energy transfer dependence at the vertex [49, 45], we use form factors of the type

$$
F_\alpha(\vec{q}\,) = \frac{\Lambda^2_{\alpha\Lambda\Lambda} - m^2_\alpha}{\Lambda^2_{\alpha\Lambda\Lambda} + \vec{q}^{\,2}}, \qquad (18)
$$

where the α symbol stands for σ or ω.

The use of the given form factor at each vertex leads to the following extended expressions for the potentials:

$$
V_\alpha(r) = V_\alpha(m_\alpha, r) - \left\{V_\alpha(z,r) - \frac{(\Lambda^2_{\alpha\Lambda\Lambda} - m^2_\alpha)}{2\Lambda_{\alpha\Lambda\Lambda}}\,\frac{\partial V_\alpha(z,r)}{\partial z}\right\}_{z=\Lambda_{\alpha\Lambda\Lambda}}. \qquad (19)
$$

Furthermore, for the $^1S_0$ channel, in which we will be interested in this work, one can replace

$$
\begin{aligned}
\vec{\sigma_1}\cdot\vec{\sigma_2} &\to -3, &(20)\\
\vec{L}\cdot\vec{S} &\to 0, &(21)\\
S_{12} &\to 0. &(22)
\end{aligned}
$$

Thus, finally and after including the above substitutions, the $\Lambda\Lambda$ potential reads

$$
V^{L=S=0}_{\Lambda\Lambda}(r) = V^{L=S=0}_\sigma(r) + V^{L=S=0}_\omega(r), \qquad (23)
$$

where

$$
V^{L=S=0}_\sigma(r) = -\frac{g^2_{\sigma\Lambda\Lambda}}{4\pi}m_\sigma\left\{\tilde{\mathbf{Y}}(\sigma,r) + \frac{1}{2m^2_\Lambda}\left[\left(\vec{\nabla}\tilde{\mathbf{Y}}(\sigma,r)\right)_L\cdot\vec{\nabla} + \tilde{\mathbf{Y}}(\sigma,r)\nabla^2\,\right]\right\}, \qquad (24)
$$

$$
\begin{aligned}
V^{L=S=0}_\omega(r) &= \frac{m_\omega}{4\pi}\left\{\hat{\mathbf{g}}^2_{\omega\Lambda\Lambda}\tilde{\mathbf{Y}}(\omega,r) + \frac{(g^2_{\omega\Lambda\Lambda} - \hat{\mathbf{g}}^2_{\omega\Lambda\Lambda})}{m^2_\omega}\frac{(\Lambda^2_{\omega\Lambda\Lambda} - m^2_\omega)^2}{2m_\omega\Lambda_{\omega\Lambda\Lambda}}e^{-\Lambda_{\omega\Lambda\Lambda}\,r}\right. \\
&- \left.\frac{3g^2_{\omega\Lambda\Lambda}}{2m^2_\Lambda}\left[\left(\vec{\nabla}\tilde{\mathbf{Y}}(\omega,r)\right)_L\cdot\vec{\nabla} + \tilde{\mathbf{Y}}(\omega,r)\nabla^2\,\right]\right\}. \qquad (25)
\end{aligned}
$$

Vertex	$g_\alpha/\sqrt{4\pi}$	$f_\alpha/\sqrt{4\pi}$	Λ_α (GeV)
$\omega\Lambda\Lambda$	2.981	-2.796	2
$\sigma\Lambda\Lambda$	2.138	$-$	1

Table 2: Coupling constants g_α, f_α and cutoff masses Λ_α found in Ref. [46] for model $\hat{A}$.

The subindex L means that the operator $\vec{\nabla}$ only acts on the function $\tilde{\mathbf{Y}}(\alpha, r)$. On the other hand, $\hat{\mathbf{g}}^2_{\omega\Lambda\Lambda}$ and $\tilde{\mathbf{Y}}(\alpha, r)$ are given by

$$\hat{\mathbf{g}}^2_{\omega\Lambda\Lambda} = g^2_{\omega\Lambda\Lambda} - \frac{1}{2}\left(\frac{m_\omega}{m_\Lambda}\right)^2 \left(\frac{3g^2_{\omega\Lambda\Lambda}}{2} + \frac{m_\Lambda}{m_N} g_{\omega\Lambda\Lambda} f_{\omega\Lambda\Lambda} + \left(\frac{m_\Lambda}{m_N}\right)^2 f^2_{\omega\Lambda\Lambda}\right), \quad (26)$$

$$\tilde{\mathbf{Y}}(\alpha, r) = Y(m_\alpha r) - \left\{1 + \frac{r}{2\Lambda_{\alpha\Lambda\Lambda}}\left(\Lambda^2_{\alpha\Lambda\Lambda} - m^2_\alpha\right)\right\} \frac{\Lambda_{\alpha\Lambda\Lambda}}{m_\alpha} Y(\Lambda_{\alpha\Lambda\Lambda} r). \quad (27)$$

The phenomenological Lagrangians of Eqs. (13) – (14) and form factors of the type of Eq. (18) have been used in Refs. [45, 46] to describe ΛN elastic scattering data[5]. The interactions of Ref. [46] are obtained from those in Ref. [45] by neglecting their small time dependence and performing again a fit to the same set of data. The NN vertices are taken from the Bonn potential [49]. The model $\hat{A}$ of Ref. [46] leads to a $\Lambda\Lambda$ potential of the same form of that of Eqs. (15) – (16) and in Table 2 we give the values of the coupling constants and cutoff masses found in this reference. Note that in Ref. [46], the strength of the $\omega\Lambda\Lambda$ coupling is fixed by means of the $SU(6)$ symmetry ($g_{\omega\Lambda\Lambda} = \frac{2}{3} g_{\omega NN}$ and $f_{\omega\Lambda\Lambda} = \frac{5}{6} f_{\omega NN} - \frac{1}{2} f_{\rho NN}$) and thus $g_{\sigma\Lambda\Lambda}$, $\Lambda_{\sigma\Lambda\Lambda}$ and $\Lambda_{\omega\Lambda\Lambda}$ are the only free parameters adjusted to the empirical data. In that reference is also pointed out that the fit has little sensitivity to the cutoff mass $\Lambda_{\sigma\Lambda\Lambda}$.

In principle, in this work the free parameters would also be the coupling constants of the σ ($g_{\sigma\Lambda\Lambda}$) and ω ($g_{\omega\Lambda\Lambda}$ and $f_{\omega\Lambda\Lambda}$) mesons to the hyperon Λ and the cutoffs ($\Lambda_{\sigma\Lambda\Lambda}$, $\Lambda_{\omega\Lambda\Lambda}$) of the corresponding form factors. However, due to the limited set of data available to this study, we fix $\Lambda_{\omega\Lambda\Lambda} = 2$ GeV and $f_{\omega\Lambda\Lambda} = -2.796$, as in Table 2. To check the sensitivity of the hypernuclear data to $g_{\omega\Lambda\Lambda}$ and $\Lambda_{\sigma\Lambda\Lambda}$, we consider different families of potentials obtained by using different values for the ratio $g_{\omega\Lambda\Lambda}/g_{\omega NN}$ above and below the $SU(6)$ prediction, 2/3, and taking for each value of the former ratio, two different values (1 and 2 GeV) of the cutoff $\Lambda_{\sigma\Lambda\Lambda}$. Thus, for each potential we are left with just one free parameter, $g_{\sigma\Lambda\Lambda}$, which is obtained from a best χ^2 fit to the values of $B_{\Lambda\Lambda}$ reported in Table 1.

As we will see, there is a strong correlation between the parameters $g_{\sigma\Lambda\Lambda}$ and $\Lambda_{\sigma\Lambda\Lambda}$, and the quantity $g_{\sigma\Lambda\Lambda} \times (1 - m^2_\sigma/\Lambda^2_{\sigma\Lambda\Lambda})$ remains constant within approximately 10%. This is due to the fact that for bound Λ particles in the double$-\Lambda$ hypernucleus, the *average* momentum transfered in the $\Lambda\Lambda$ vertex is much smaller than the typical values ($\approx$ 1

[5]In these references, it is not only studied the $\Lambda N \to \Lambda N$ process, but all hyperon-nucleon reaction channels measured experimentally ($\Lambda N \to \Lambda N$, $\Sigma N \to \Lambda N'$ and $\Sigma N \to \Sigma' N'$) using a coupled channel formalism.

GeV) of the cutoff mass. In these circumstances the form factor at the $\sigma\Lambda\Lambda$ vertex can be approximated by

$$F_\sigma(\vec{q}\,) = 1 - \frac{m_\sigma^2}{\Lambda_{\sigma\Lambda\Lambda}^2} + \mathcal{O}\left(\frac{\vec{q}^{\,2}}{\Lambda_{\sigma\Lambda\Lambda}^2}\right). \tag{28}$$

Similar conclusions can be drawn in the case of $g_{\omega\Lambda\Lambda}$ and $\Lambda_{\omega\Lambda\Lambda}$.

Finally, we would like to mention that the $\Lambda\Lambda$ interaction determined in this work corresponds to an effective interaction in the nuclear medium and it is not directly comparable with that of Ref. [46]. We will come back to this point in Subsect. 4.7.

2.2 Model for the Λ-Core Interaction

The detailed study of the Λ-nuclear core dynamics is not the aim of this paper. However, we need to check the sensitivity of the parameters of the $\Lambda\Lambda$ interaction, obtained from an overall fit to the available $B_{\Lambda\Lambda}$ data, to the used Λ-nuclear core potential. Thus, we have considered different Λ-nucleus potentials suggested in the literature, which have been adjusted to reproduce the binding energies B_Λ of the single–Λ hypernuclei ground states.

In this subsection we will give details of the different Λ-core potentials used through this work. All except for one are obtained from models to describe the dynamics of the ΛN system. To obtain a Λ-nucleus potential ($\mathcal{V}_{\Lambda A}$) from a ΛN interaction ($V_{\Lambda N}$) we fold the latter with the corresponding nuclear density of the core. For closed–shell nuclear cores and Λ particles in the ground state ($1s^{\frac{1}{2}}$), all the couplings involving the total angular momentum $\vec{L}$ or spin couplings of the type $\vec{\sigma_1}\cdot\vec{\sigma_2}$ or S_{12} in the $V_{\Lambda N}$ potential do not contribute, and thus for this particular scenario the $\mathcal{V}_{\Lambda A}$ potential is given by

$$\mathcal{V}_{\Lambda A}(r) = \int d^3r' \rho_c(|\vec{r} - \vec{r}\,'|) V_{\Lambda N}(r'), \tag{29}$$

where ρ_c corresponds to the density for the centers of nucleons which is obtained from the charge density by taking into account the finite size of the nucleon (for details see Sect. 4 of Ref. [68]).

A considerable amount of work has been devoted to the study of the mesonic decay of the hypernucleus ${}^{5}_{\Lambda}$He as a mean to investigate the repulsive part of the ΛN interaction. Then, different types of Λ-^{4}He potentials have been suggested in the literature [22, 29]. Among them we have selected two potentials, with (YNG) and without (ORG) a repulsive part in the elementary ΛN interaction. These potentials are determined by the following ΛN interactions:

$$V_{\Lambda N}(r)^{ORG} = -38.19\, e^{-(r/1.034)^2}\ \text{MeV}, \tag{30}$$

$$V_{\Lambda N}(r)^{YNG} = \left[919\, e^{-(r/0.5)^2} - 206.54\, e^{-(r/0.9)^2} - 9.62\, e^{-(r/1.5)^2}\right]\ \text{MeV}. \tag{31}$$

In all cases r is given in fermis. The parameters of the above interactions have been adjusted to reproduce the ground state binding energy of the ${}^{5}_{\Lambda}$He [22].

To perform a simultaneous analysis of the three double−Λ hypernuclei we are interested in, we have also considered other two Λ-core potentials.

- In the spirit of the previous subsection for the $\Lambda\Lambda$ dynamics, the first Λ-core potential (SW) considered here, is obtained from an effective $\sigma-\omega$ exchange model to describe the ΛN interaction given by

$$V^{\sigma}_{\Lambda N}(m_\sigma, r) = -\frac{\bar{g}_{\sigma\Lambda\Lambda} g_{\sigma NN}}{4\pi} m_\sigma Y(m_\sigma r), \tag{32}$$

$$\begin{aligned} V^{\omega}_{\Lambda N}(m_\omega, r) &= \frac{m_\omega}{4\pi}\left\{\bar{g}_{\omega\Lambda\Lambda} g_{\omega NN} - \frac{1}{4}\left(\frac{m_\omega^2}{m_\Lambda m_N}\right)\right. \\ &\times \left.\left(\bar{g}_{\omega\Lambda\Lambda} g_{\omega NN} - \frac{m_\Lambda}{m_N}\bar{g}_{\omega\Lambda\Lambda} f_{\omega NN} - g_{\omega NN}\bar{f}_{\omega\Lambda\Lambda}\right)\right\} Y(m_\omega r). \end{aligned} \tag{33}$$

The potential above is a simplified version of the more general one described in Eqs. (38) – (39) of Ref. [43]. Firstly, as we will mention below, we use monopolar type form factors instead of Gaussian type form factors as it is done there. Secondly, we have neglected all terms of order $\mathcal{O}\left((m_{\rm meson}/m_{\rm baryon})^4\right)$ and also all terms of order $\mathcal{O}\left(m^2_{\rm meson}(m^2_\Lambda - m^2_N)/m^4_{\rm baryon}\right)$. Thirdly, we have neglected all type of spin terms which will not contribute for closed–shell nuclear cores and Λ particles in the ground state ($1s^{\frac{1}{2}}$). Finally, we have neglected non-local terms of the potential which would be proportional to the Λ momentum squared over the product of the Λ and nucleon masses ($\cdots(\nabla^2\phi_\Lambda(\vec{r}))/4m_\Lambda m_N$). For a bound particle, one expects these contributions to be quite small.

We do not consider potentials due to the exchange of strange mesons (K, K^*, $\cdots$), which though relevant to describe the ΛN scattering process [43, 46], contribute to the binding energy only as Fock terms and thus are suppressed at least by a $1/A$ factor. In Ref. [14] these Fock contributions were evaluated and found to be small.

To take into account the finite size of the baryons involved at the vertices, monopolar form factors are used here as well. In coordinate space the inclusion of form factors is implemented by means of the substitution [49]

$$\begin{aligned} V^{\alpha}_{\Lambda N}(r) &= V^{\alpha}_{\Lambda N}(m_\alpha, r) - \frac{\Lambda^2_{\alpha NN} - m^2_\alpha}{\Lambda^2_{\alpha NN} - \Lambda^2_{\alpha\Lambda\Lambda}} V^{\alpha}_{\Lambda N}(\Lambda_{\alpha\Lambda\Lambda}, r) \\ &+ \frac{\Lambda^2_{\alpha\Lambda\Lambda} - m^2_\alpha}{\Lambda^2_{\alpha NN} - \Lambda^2_{\alpha\Lambda\Lambda}} V^{\alpha}_{\Lambda N}(\Lambda_{\alpha NN}, r), \end{aligned} \tag{34}$$

where the α symbol stands for σ or ω. Thus, finally the ΛN potential reads

$$V^{\rm SW}_{\Lambda N}(r) = V^{\sigma}_{\Lambda N}(r) + V^{\omega}_{\Lambda N}(r). \tag{35}$$

In principle, the couplings $g_{\omega\Lambda\Lambda}$, $g_{\sigma\Lambda\Lambda}$ and $f_{\omega\Lambda\Lambda}$ introduced in Eqs. (15) – (16) should coincide with those appearing in Eqs. (32) – (33), and denoted there with an overline. However, these couplings might be significantly different, because in both cases we are dealing with effective interactions ($\Lambda\Lambda$ or ΛN) which parameters

Vertex	$g_\alpha/\sqrt{4\pi}$	$f_\alpha/\sqrt{4\pi}$	Λ_α (GeV)
ωNN	4.472	0	1.5
σNN	2.385	–	1.7

Table 3: Coupling constants g_α, f_α and cutoff masses Λ_α for the NN vertices. Values are taken from Ref. [49].

also account for some contributions ($\phi-$exchange, intermediate states: ΞN, ΣN, etc..) not explicitly included. Furthermore, these effective interactions are affected by renormalization effects due to the nuclear medium, which could be significantly different for each interaction. On top of that, as we mentioned above, some non-localities and Fock contributions have been neglected in the treatment of the Λ-core interaction, and their effect, though presumably small, could affect the value of the effective couplings in Eqs. (32) – (33). Thus, to avoid confusions with the $\Lambda\Lambda$ couplings, we denote with an overline those couplings which appear in the ΛN potential.

In Eqs. (33) – (34) we fix the $\omega\Lambda\Lambda$ coupling parameters to the values given above in Table 2. The ωNN and σNN coupling parameters are taken from the Bonn potential [49] and compiled here in Table 3. Finally, for each hypernucleus $({}^{A+1}_{\Lambda}Z)$ we fit $\bar{g}_{\sigma\Lambda\Lambda}$ to reproduce the ground state binding energy, using two values, 1 (SW1) and 2 GeV (SW2), for the cutoff parameter $\Lambda_{\sigma\Lambda\Lambda}$, as we discussed in the previous subsection.

- The second Λ-nuclear core potential (BOY) considered, is phenomenological and it is not based on any model for the ΛN interaction. It was suggested long time ago for medium nuclei by A. Bouyssy [13]. It has only one parameter, V_0, which we adjust for each hypernucleus $({}^{A+1}_{\Lambda}Z)$ to reproduce the ground state binding energy. The potential reads:

$$\begin{aligned} \mathcal{V}^{\rm BOY}_{\Lambda A}(r) &= \frac{V_0}{1+e^{(r-R)/a}}\,, \\ R &= 1.1\,{\rm A}^{\frac{1}{3}}\ {\rm fm},\ \ a = 0.6\ {\rm fm}. \end{aligned} \tag{36}$$

A similar potential was also suggested in Ref. [19]. There, it is also shown that, despite of not including a spin$-$orbit part, these type of potentials give also reasonable descriptions of non **s**-wave Λ bound states, in agreement with the previous findings of Ref. [12].

3 Mesonic Decay of Double$-\Lambda$ Hypernuclei

The mesonic decay has been computed following the method exposed in Refs. [20] and [30] which uses shell-model baryon wave functions and distorted pion waves. For light nuclei

in the p shell, as boron, the low lying state structure might not be correctly represented simply by *unoccupied* single–particle orbitals, and a residual interaction of the Cohen-Kurath type [67] has been added. Reviews on the subject can be found in Refs. [34] and [41]. We compute the decay widths corresponding to the following processes

$$
\begin{aligned}
{}^{A+2}_{\Lambda\Lambda}\mathrm{Z} &\rightarrow \left({}^{A+2}_{\Lambda}\mathrm{Z}\right)_b + \pi^0, && (37)\\
{}^{A+2}_{\Lambda\Lambda}\mathrm{Z} &\rightarrow \left({}^{A+2}_{\Lambda}(\mathrm{Z}+1)\right)_b + \pi^-, && (38)\\
{}^{A+2}_{\Lambda\Lambda}\mathrm{Z} &\rightarrow \left({}^{A+1}_{\Lambda}\mathrm{Z}\right)_{gs} + n + \pi^0, && (39)\\
{}^{A+2}_{\Lambda\Lambda}\mathrm{Z} &\rightarrow \left({}^{A+1}_{\Lambda}\mathrm{Z}\right)_{gs} + p + \pi^-, && (40)
\end{aligned}
$$

where b denotes that the remaining Λ is in the ground state and the outgoing nucleon is in an unoccupied bound state of the daughter hypernucleus. On the other hand gs means that the daughter hypernucleus is left on its ground state. In the two last reactions the outgoing nucleon goes to the continuum.

We use a model in which the pionic decay is produced by a one-body operator

$$
\delta\widetilde{H}_{\Lambda\pi N} = -Gm_\pi^2 \left\{ S - (\frac{P}{m_\pi})\, \vec{\sigma}\cdot\vec{q} \right\} \tau^\lambda, \tag{41}
$$

where $(Gm_\pi^2)^2/8\pi = 1.945\,10^{-15}$, the constants S and P are equal to 1.06 and 0.527 respectively and m_π is the pion mass (139.6 or 135.0 MeV for π^- or π^0). Finally, $\vec{q}$ is the momentum of the outgoing pion and the Pauli matrices $\vec{\sigma}$ and τ^λ act on the spin and isospin Hilbert spaces respectively. The τ^λ operator in Eq. (41) implements the $\Delta T = 1/2$ rule by means of which the rate of $\Lambda \rightarrow \pi^- p$ is twice as large as that of $\Lambda \rightarrow \pi^0 n$.

The vacuum Λ decay width is readily evaluated and leads for proton or neutron decay to

$$
\begin{aligned}
\Gamma^{(\alpha)}_{free} &= C^{(\alpha)}\, \frac{(Gm_\pi^2)^2}{4\pi} \frac{m_N\, q_{cm}}{m_\Lambda} \left\{ S^2 + \left(\frac{P}{m_\pi}\right)^2 q_{cm}^2 \right\}, && (42)\\
q_{cm} &= \frac{\lambda^{1/2}(m_\Lambda^2, m_N^2, m_\pi^2)}{2m_\Lambda}, && (43)\\
\lambda(x,y,z) &= x^2 + y^2 + z^2 - 2xy - 2xz - 2yz, && (44)
\end{aligned}
$$

with the isospin coefficients $C^{(p)} = 4$ and $C^{(n)} = 2$, and q_{cm} the pion momentum in the center of mass frame. One can see from Eq. (42) that the parity violating term, S, is the dominant one in the decay.

To illustrate the main ingredients entering in the decay, we reproduce below the decay width for any of the processes of Eqs. (37) – (40), in the simple shell–model case where the spin–orbit splitting of the nuclear–core levels is not taken into account:

$$
\begin{aligned}
\Gamma^{(\alpha)} &= C^{(\alpha)} \sum_{N\neq F} \int \frac{d^3q}{(2\pi)^3} \frac{1}{2\omega(q)} 2\pi\delta(m_\Lambda - B_{\Lambda\Lambda} + B_\Lambda - \omega(q) - E_N)(Gm_\pi^2)^2 \\
&\times \left\{ S^2 \left| \int d^3x_1 \left[\int d^3x_2 \mathbf{\Phi_{\Lambda\Lambda}}(\vec{x_1},\vec{x_2}) \varphi^*_\Lambda(\vec{x_2}) \right] \widetilde{\varphi}^{(-)}_\pi(\vec{q},\vec{x_1})^* \varphi^*_N(\vec{x_1}) \right|^2 \right. \\
&+ \left. \left(\frac{P}{m_\pi}\right)^2 \left| \int d^3x_1 \left[\int d^3x_2 \mathbf{\Phi_{\Lambda\Lambda}}(\vec{x_1},\vec{x_2}) \varphi^*_\Lambda(\vec{x_2}) \right] \vec{\nabla}_1 \widetilde{\varphi}^{(-)}_\pi(\vec{q},\vec{x_1})^* \varphi^*_N(\vec{x_1}) \right|^2 \right\}, \qquad (45)
\end{aligned}
$$

where φ_N and E_N are the wave function and energy of the outgoing nucleon in the Λ decay, $\mathbf{\Phi_{\Lambda\Lambda}}$ is the wave–function of the $\Lambda\Lambda$ pair, φ_Λ is the Λ wave function in the daughter hypernucleus, $\omega(q)$ the pion energy, and the sum over N runs over the unoccupied nuclear orbitals given by n and l since spin sums are already performed. In Eq. (45) the sums over N are over proton or neutron orbitals according to α. Note that if the $\Lambda\Lambda$ interaction and the HE term were neglected and if $B_{\Lambda\Lambda}$ were replaced by $2B_\Lambda$ in the energy conservation delta, then Eq. (45) would yield a width of twice the corresponding one for the decay of a Λ in a single–Λ-hypernucleus.

The corresponding expression for the decay width when the spin–orbit splitting of the nuclear–core levels is considered, can be easily deduced from Eqs. (6)-(15) of Ref. [20].

The pion wave function ($\widetilde{\varphi}_\pi^{(-)}(\vec{q},x)^*$) as a block corresponds to an incoming solution of the Klein Gordon equation,

$$\left[-\vec{\bigtriangledown}^2 + m_\pi^2 + 2\omega(q)V_{\rm opt}(\vec{x})\right]\widetilde{\varphi}_\pi^{(-)}(\vec{q},\vec{x})^* = (\omega(q) - V_C(\vec{x}))^2\widetilde{\varphi}_\pi^{(-)}(\vec{q},\vec{x})^*, \qquad (46)$$

with $V_C(\vec{x})$ the Coulomb potential created by the nucleus considering finite size and vacuum polarization effects and $V_{\rm opt}(\vec{x})$ the optical potential which describes the π-nucleus interaction. This potential has been developed microscopically and it is presented in detail in Refs. [68, 69]. It contains the ordinary lowest order optical potential pieces constructed from the s– and p–wave πN amplitudes. In addition second order terms in both s– and p–waves, responsible for pion absorption, are also considered. Standard corrections, as second-order Pauli re-scattering term, ATT term, Lorentz–Lorenz effect and long and short range nuclear correlations, are also taken into account. This theoretical potential reproduces fairly well the data of pionic atoms (binding energies and strong absorption widths) [68] and low energy π-nucleus scattering [69].

The Λ wave function in the daughter hypernucleus, φ_Λ, is computed using the Λ-core potentials described in Subsect. 2.2. For the nucleons we have used the following potential [70]

$$V(r) \;=\; \frac{-50\ \text{MeV}}{1+\exp[(r-R)/a]}, \qquad (47)$$

with $R = 1.25A^{1/3}$ fm, $a = 0.65$ fm, which provides a fair reproduction of the nuclear levels for the average energy of major shells, as well as realistic nucleon wave functions.

Because, the strength of the spin–orbit force is small in the boron region (about 4 MeV), we will neglect it, and to calculate the mesonic decay of the ${}^{13}_{\Lambda\Lambda}$B hypernucleus we will use the potential of Eq. (47) and Cohen-Kurath spectroscopic factors [71] for the $1p-$shell. Those are obtained from effective interactions for the $1p-$shell deduced in Ref. [67] by fitting different nuclear energy levels. Thus, the contribution to the mesonic width of the processes where the outgoing nucleon is trapped in the $1p-$shell is computed as follows. The initial state consists of seven nucleons in the $1p-$configuration[6] plus two

[6]The $1s_{\frac{1}{2}}-$shell is full, and it behaves, in a very good approximation, as an inert core [72].

Λ hyperons coupled to $L = 0 = S$, whereas the final state consists of eight nucleons in the $1p-$configuration plus a Λ hyperon and a pion. The transition operator annihilates a Λ hyperon and creates a nucleon in the $1p-$configuration. To compute the nuclear matrix elements involved in the mesonic decay, one needs the angular momentum–isospin reduced matrix element of the nucleon creation operator, $a^\dagger_\rho$, between fully antisymmetric states of n and $n-1$ nucleons in the angular momentum–isospin configuration ρ and coupled respectively to Γ_R and Γ_i angular momentum and isospin quantum numbers. This is given by [73],

$$\frac{\langle \rho^n \Gamma_R ||| a^\dagger_\rho ||| \rho^{n-1} \Gamma_i \rangle}{\sqrt{n}\sqrt{2\Gamma_R + 1}} \;=\; \langle \rho^n \Gamma_R | \} \rho^{n-1} \Gamma_i \rangle, \tag{48}$$

where the reduced matrix element is defined by Eq. (A.3.a17) of Ref. [73] and $\langle ... | \} ... \rangle$ are the coefficients of fractional parentage. They are related to the spectroscopic factors, $\mathcal{S}$, by

$$\mathcal{S}(\Gamma_R; \Gamma_i, \rho) \;=\; n \, \langle \rho^n \Gamma_R | \} \rho^{n-1} \Gamma_i \rangle^2. \tag{49}$$

After a little of Racah-algebra, one finds that the averaged modulus squared of the nuclear matrix element ($\mathcal{M}$) which determines the $1p-$shell contribution to the decay processes of Eqs. (37) – (38) is given by

$$\begin{aligned}
&\overline{\sum_i} \sum_f |\mathcal{M}|^2 = \\
&\sum_{J_R, T_R, \alpha_R, j} \frac{2J_R + 1}{(2J_i + 1)(2j + 1)} \mathcal{C}(T_i, \frac{1}{2}, T_R | \tau_i, \tau_R - \tau_i, \tau_R)^2 \mathcal{S}(J_R, T_R, \alpha_R; J_i, T_i, \mathrm{gs}, j) \\
&\times \sum_{m, m_{\Lambda_s}} \left| \left\langle \Lambda \, \frac{1}{2} \, m_{\Lambda_s} | \delta \widetilde{H}_{\Lambda \pi N} | N j m, \frac{1}{2}(\tau_R - \tau_i) \otimes \pi \, \vec{q}\,(\alpha_R) \right\rangle \right|^2
\end{aligned} \tag{50}$$

where $J_i = 3/2, T_i = 1/2$ and $\tau_i = -1/2$ are the total angular momentum, isospin and third isospin component quantum numbers of the initial nuclear core (^{11}B), J_R, T_R and $\tau_R = 0$ for π^- decay or -1 for π^0 decay, are the corresponding quantum numbers for the final nuclear core. In addition gs and α_R stand for the ground state energy of the ^{11}B core and the excitation energy of the final cores ^{12}B* or ^{12}C* and $\mathcal{C}$ is a Clebsch–Gordan coefficient. On the other hand j, m and $\tau_R - \tau_i$ determines the wave function of the outgoing nucleon after the decay. The sum over the "R" quantum numbers gives us the sum over $p-$shell excited states in the final nuclear core. For π^- (π^0) decay, we sum the contribution of the eighteen (eight) excited states which spectroscopic factors and energies are given in Table 1[7] (label: "Stripping for target $A = 11$ $(\frac{3}{2}, \frac{1}{2})$") of Ref. [71]. Finally, $|\pi \, \vec{q}\,(\alpha_R)\rangle$ and $|\Lambda m_{\Lambda_s}\rangle$ stand for the pion wave function in the continuum, being its momentum determined by energy conservation, and the spectator Λ wave function, being its spatial wave-function determined by the projection

[7]Note that in this table the origin of energies is that of the ^{12}C ground state.

$$\langle\varphi_\Lambda(\vec{x}_2)|\Phi_{\Lambda\Lambda}(\vec{x}_1,\vec{x}_2)\rangle \;=\; \int d^3x_2 \mathbf{\Phi_{\Lambda\Lambda}}(\vec{x}_1,\vec{x}_2)\varphi^*_\Lambda(\vec{x}_2). \tag{51}$$

The matrix element of the interaction $\delta\widetilde{H}_{\Lambda\pi N}$ in Eq. (50) is of the same type of that given in Eqs. (6)-(15) of Ref. [20].

Further details of the calculation of the mesonic decay width as the treatment of the outgoing nucleons in the continuum, the correct energy balance in the reaction, the correct treatment of the quasielastic collisions of the outgoing pion, the procedure to perform the d^3q and $d\Omega_1$ integrations, etc., can be found in Ref. [30].

Experimentally, what can be observed are the inclusive processes

$$^{A+2}_{\Lambda\Lambda}\mathrm{Z} \;\rightarrow\; X + \Lambda + \pi^0, \tag{52}$$
$$^{A+2}_{\Lambda\Lambda}\mathrm{Z} \;\rightarrow\; X + \Lambda + \pi^-. \tag{53}$$

The main contribution to these processes is given by the exclusive ones shown in Eqs. (37) – (40). This can be seen by looking at the overlap integral defined in Eq. (51), which appears in Eq. (45). If one uses HF wave functions for the $\Lambda\Lambda$ pair and the pure spectator approximation, in which the monoparticle wave function used to construct $\mathbf{\Phi^{HF}_{\Lambda\Lambda}}$ coincides with that of the Λ ground state in the daughter hypernucleus, then, due to the orthogonality of the Λ wave functions, only those processes where the non-decaying Λ in the daughter hypernucleus remains in the ground state will contribute. Even if these approximations are not used, we have checked that those processes included in Eqs. (52) – (53) and not included in Eqs. (37) – (40) represent less than 2-3% of the total. Therefore, in what follows we will approximate the inclusive double$-\Lambda$ hypernucleus mesonic decay widths (to π^0 or to π^-) by those corresponding to the processes specified in Eqs. (37) – (40).

4 Results

Before we start discussing the results concerning double$-\Lambda$ hypernuclei, we show briefly the results for the Λ-core potentials described in the Subsect. 2.2.

4.1 Λ-Core Potentials

We have studied not only the three experimentally observed double$-\Lambda$ hypernuclei. To study the A dependence of $\Delta B_{\Lambda\Lambda}$ and the mesonic decay width, we have also considered the nuclear core closed–shell hypernuclei $^{42}_{\Lambda\Lambda}$Ca, $^{92}_{\Lambda\Lambda}$Zr and $^{210}_{\Lambda\Lambda}$Pb. Unfortunately, the binding energies of the corresponding single–Λ hypernuclei ($^{41}_{\Lambda}$Ca, $^{91}_{\Lambda}$Zr and $^{209}_{\Lambda}$Pb) are not known and we have had to approximate them by the binding energies of the closest hypernuclei known experimentally. Thus, we have used the experimental binding energies corresponding to $^{40}_{\Lambda}$Ca, $^{89}_{\Lambda}$Y and $^{208}_{\Lambda}$Pb. In Table 4 the binding energies, Λ-core reduced

Hypernucleus	B_Λ^{exp} [MeV]	density	A	$R\,(c)$ [fm]	$\alpha\,(a$ [fm])	μ_A (MeV)
${}^{5}_{\Lambda}$He	3.12±0.02 [1], [2]	HO	4	1.358	0	858.6
${}^{9}_{\Lambda}$ Be	6.71±0.04 [1]	HO	8	1.77	0.631	970.4
${}^{12}_{\Lambda}$ B	11.37±0.06 [1]	HO	11	1.69	0.811	1006.1
${}^{40}_{\Lambda}$ Ca	18.7± 1.1 [3]					
${}^{41}_{\Lambda}$ Ca		2pF	40	3.51	0.563	1083.17
${}^{89}_{\Lambda}$ Y	22.0± 0.5 [4]					
${}^{91}_{\Lambda}$ Zr		2pF	90	4.84	0.55	1100.95
${}^{208}_{\Lambda}$ Pb	26.5± 0.5 [4]					
${}^{209}_{\Lambda}$ Pb		2pF	208	6.624	0.549	1109.21

Table 4: Binding energies, charge densities ([74]), nuclear mass numbers, and Λ-core reduced masses for several single–Λ hypernuclei used through this work. 2pF stands for a two parameter Fermi density, $\rho_{\rm 2pF}(r) = \rho_0/\left(1+e^{(r-c)/a}\right)$, and HO stands for an harmonic oscillator density, $\rho_{\rm HO}(r) = \rho_0\left(1+\alpha\,(r/R)^2\right)e^{-(r/R)^2}$. The density of nucleon centers, which appears in Eq. (29), is obtained from the charge density by taking into account the finite size of the nucleon (for details see Sect. 4 of Ref. [68]).

masses and details of the charge densities for all single–Λ hypernuclei considered in this work can be found.

In Table 5, we show the binding energies and mean squared radius obtained for the ground state of different single–Λ hypernuclei by using the Λ-core potentials described in Subsect. 2.2. In this table we also give the parameters V_0 and $\bar{g}_{\sigma\Lambda\Lambda}$ fitted to the ground state binding energy for each hypernucleus. We would like to make a few remarks:

- YNG and ORG potentials were only adjusted in Ref. [22] for ${}^{5}_{\Lambda}$He. Thus, we will restrict their use only to the case of helium.
- In the original work of Ref. [13] an overall fit to light-medium hypernuclei was performed which provided a value of $V_0 = -32 \pm 2$ MeV, which is in good agreement with the values shown in Table 5.
- One might think that for the case of the $\sigma - \omega$ interaction with a cutoff $\Lambda_{\sigma\Lambda\Lambda} =$ 1 GeV, the fitted parameter $\bar{g}_{\sigma\Lambda\Lambda}/\sqrt{4\pi}$ should coincide with the value found in Ref. [46], 2.138, for hyperon-nucleon scattering in the vacuum. We find significantly different values, 3.1-3.5, which may be due to the fact that we are dealing with a medium interaction, that we have neglected Fock terms and some non-localities which may be significant for light and heavy nuclei respectively, that we are using a Λ-core potential designed for closed–shell cores, for some hypernuclei where this

is not the case, and finally that we have not explicitly considered here the channel[8] $\Lambda N \to \Sigma N$ which is included in the analysis of Ref. [46]. To trace back the origin of this discrepancy is even more complicated when one realizes that, in both this work and that of Ref. [46], for a given set of $\omega-$couplings, what is determined is the product of $g_{\sigma\Lambda\Lambda} g_{\sigma NN}$ rather that the $g_{\sigma\Lambda\Lambda}-$ coupling alone. Hence, the observed discrepancy could also be due to differences between the σNN coupling in the vacuum and inside of the nuclear medium.

- In contrast to the findings of Ref. [46], our fits depend appreciably on the cutoff parameter $\Lambda_{\sigma\Lambda\Lambda}$. Indeed we find that the quantity $\bar{g}_{\sigma\Lambda\Lambda} \times (1 - m_\sigma^2/\Lambda_{\sigma\Lambda\Lambda}^2)$ remains constant within approximately 2%, as we expected from our discussion in Eq. (28). Despite of the fact that the latter quantity remains almost constant, for very light hypernucleus as ${}^{5}_{\Lambda}$He, the short-distance behavior of the potential depends strongly on the specific value of the cutoff $\Lambda_{\sigma\Lambda\Lambda}$, as can be seen in Fig. 1.

- Because of the folding in Eq. (29), the repulsive or attractive character at short distances of the ΛN interaction can be appreciably seen in the Λ-core potential only for very light hypernuclei as ${}^{5}_{\Lambda}$He. This is clearly shown in Fig. 1, where one can also see that for medium and heavy hypernuclei none of the Λ-core potentials provide repulsion at short distances despite of the fact that some of them are being constructed out of ΛN potentials with repulsive cores.

- For $\sigma - \omega$ type potentials, there is a strong cancelation between both components of the interaction which is translated into a great sensitivity of the binding energy to very small changes of the coupling constants, as the extremely small statistical errors of the parameter $\bar{g}_{\sigma\Lambda\Lambda}$ in Table 5 indicate.

4.2 $\Lambda\Lambda$ Interaction: HF Results

In Table 6 we show, within the HF scheme, the parameter $g_{\sigma\Lambda\Lambda}$ obtained from a best fit to the available $B_{\Lambda\Lambda}$ experimental data (Table 1). The value of the $\omega\Lambda\Lambda$ coupling is kept fixed to $g_{\omega\Lambda\Lambda} = 2g_{\omega NN}/3$ and we consider several Λ-core potentials and cutoff parameters $\Lambda_{\sigma\Lambda\Lambda}$. The χ^2 by degree of freedom for each fit is also shown. YNG and ORG potentials have been considered only for helium.

The fits using the ORG for helium and BOY for beryllium and boron $\Lambda-$core interactions, provide the best χ^2/dof (≈ 0.1) among all $\Lambda-$core interactions considered. Anyhow, most of the fits presented in Table 6 with different $\Lambda-$core interactions are statistically acceptable, and in all the cases the differences in $g_{\sigma\Lambda\Lambda}$ from the different fits are of the order of the statistical errors. Indeed, the fitted values of $g_{\sigma\Lambda\Lambda}$ only depends significantly on the value of the cutoff parameter $\Lambda_{\sigma\Lambda\Lambda}$. Thus, the ambiguities in the

[8]Though relevant far beyond the ΛN threshold, we expect the contribution of this new channel to be small for Λ-bound states because of Pauli-blocking [32]. In any case it will contribute to the above-mentioned difference between the $g_{\sigma\Lambda\Lambda}$ couplings.

$\Lambda_{\sigma\Lambda\Lambda}$ [GeV] Hypernucleus		YNG	ORG	BOY	SW1 1	SW2 2
${}^{5}_{\Lambda}$He	B_Λ [MeV]	3.12	3.10	3.12(2)	3.12(2)	3.12(2)
	$\langle r^2\rangle^{1/2}$[fm]	3.16	2.77	3.02(1)	3.12(1)	3.00(1)
	par: $-V_0$ or $\hat{g}_{\sigma\Lambda\Lambda}$			29.95(6)	3.4916(11)	2.5662(7)
${}^{9}_{\Lambda}$Be	B_Λ [MeV]			6.71(4)	6.71(4)	6.71(4)
	$\langle r^2\rangle^{1/2}$[fm]			2.46(1)	2.61(1)	2.533(5)
	par: $-V_0$ or $\hat{g}_{\sigma\Lambda\Lambda}$			28.02(7)	3.4389(16)	2.5436(12)
${}^{12}_{\Lambda}$ B	B_Λ [MeV]			11.37(6)	11.37(6)	11.37(6)
	$\langle r^2\rangle^{1/2}$[fm]			2.216(3)	2.259(4)	2.183(3)
	par: $-V_0$ or $\hat{g}_{\sigma\Lambda\Lambda}$			31.98(10)	3.3938 (14)	2.506(1)
${}^{41}_{\Lambda}$ Ca	B_Λ [MeV]			18.7 ± 1.1	18.7 ± 1.1	18.7 ± 1.1
	$\langle r^2\rangle^{1/2}$[fm]			2.47(3)	2.21(3)	2.26(3)
	par: $-V_0$ or $\hat{g}_{\sigma\Lambda\Lambda}$			29.7 ± 1.3	3.194(16)	2.390(12)
${}^{91}_{\Lambda}$ Zr	B_Λ [MeV]			22.0(5)	22.0(5)	22.0(5)
	$\langle r^2\rangle^{1/2}$[fm]			2.91(1)	2.562(7)	2.645(8)
	par: $-V_0$ or $\hat{g}_{\sigma\Lambda\Lambda}$			28.9(5)	3.129(7)	2.353(5)
${}^{209}_{\Lambda}$ Pb	B_Λ [MeV]			26.5(5)	26.5(5)	26.5(5)
	$\langle r^2\rangle^{1/2}$[fm]			3.588(7)	3.341(5)	3.428(5)
	par: $-V_0$ or $\hat{g}_{\sigma\Lambda\Lambda}$			30.7(5)	3.145(7)	2.371(5)

Table 5: Binding energies and Λ-mean squared radius obtained for the ground state of different single–Λ hypernuclei by using the Λ-core potentials described in Eqs. (30), (31), (35) and (36). In the case of the YNG and ORG potentials , we use the parameters given in Eqs. (30) and (31). For the BOY potential we fit the parameter V_0 (MeV) in Eq. (36) whereas for the SW1 and SW2 potentials, the best fit parameter is $\hat{g}_{\sigma\Lambda\Lambda} = \bar{g}_{\sigma\Lambda\Lambda}/\sqrt{4\pi}$ in Eq. (32). The errors (in brackets) in the fit parameters and in the mean squared radius are due to the experimental errors in the binding energies which are being fitted to.

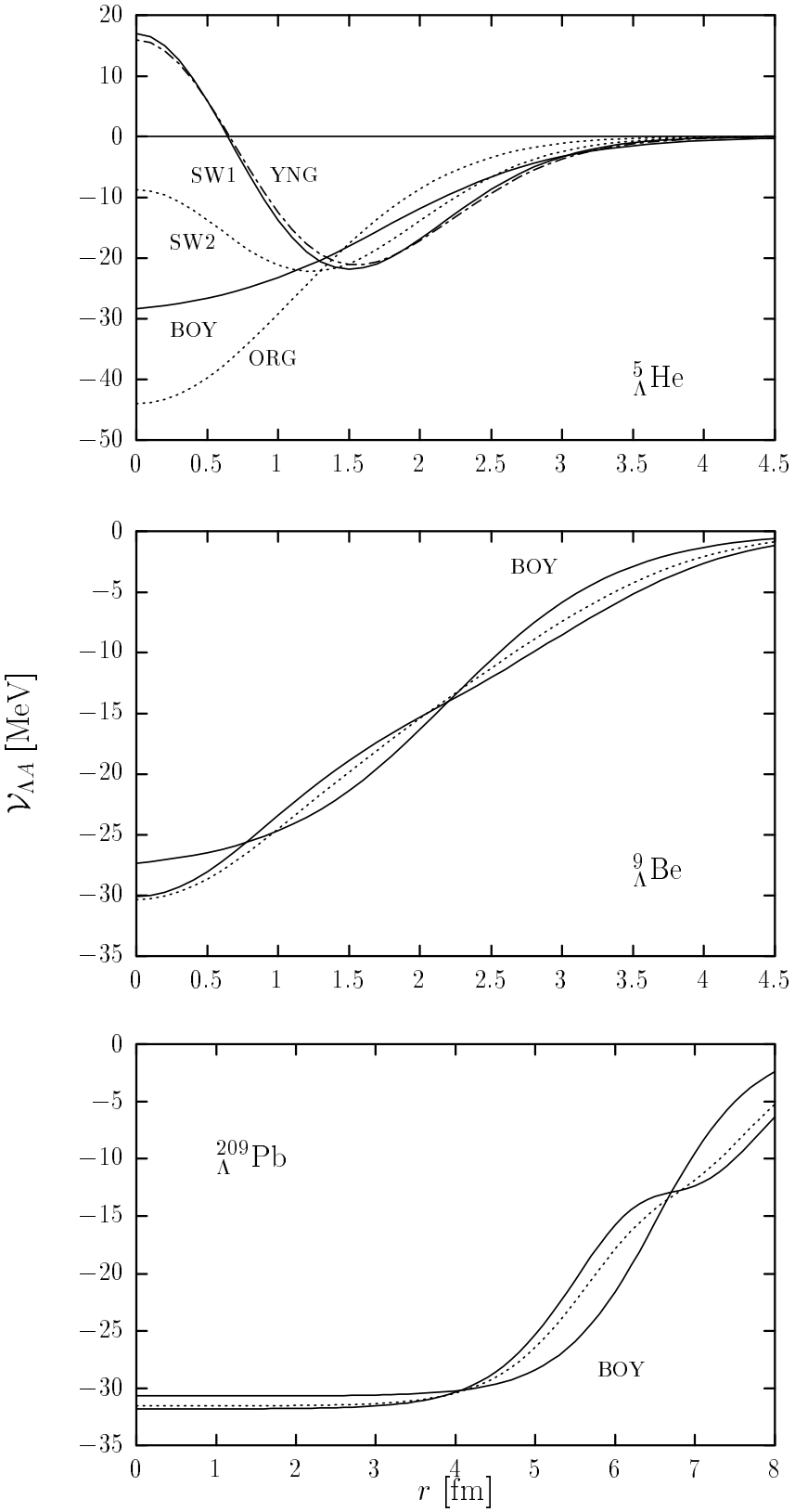

Figure 1: Λ-core potentials (in MeV) for different hypernuclei. Solid lines correspond always to the BOY or SW1 potentials. For $^{9}_{\Lambda}$Be and $^{209}_{\Lambda}$Pb, the dotted lines stands for the SW2 potential, and for $^{5}_{\Lambda}$He we also give the YNG and ORG potentials.

Λ-core potential		ΛΛ Interaction		
^{4}He	^{8}Be - ^{11}B	$\Lambda_{\sigma\Lambda\Lambda}$ (GeV)	$g_{\sigma\Lambda\Lambda}/\sqrt{4\pi}$	χ^2/dof
BOY	BOY	1	3.23 ± 0.03	1.2
ORG	BOY	1	3.22 ± 0.03	0.09
YNG	BOY	1	3.23 ± 0.03	3.0
SW1	SW1	1	3.27 ± 0.03	2.4
ORG	SW1	1	3.25 ± 0.03	0.4
YNG	SW1	1	3.27 ± 0.03	2.7
BOY	BOY	2	2.37 ± 0.02	1.3
ORG	BOY	2	2.36 ± 0.02	0.03
YNG	BOY	2	2.37 ± 0.02	3.6
SW2	SW2	2	2.37 ± 0.02	2.1
ORG	SW2	2	2.36 ± 0.02	0.6
YNG	SW2	2	2.37 ± 0.02	4.1

Table 6: HF results for $g_{\sigma\Lambda\Lambda}$ obtained from a best fit to the $B_{\Lambda\Lambda}$ data. The several rows correspond to different Λ-core potentials and different values of the cutoff $\Lambda_{\sigma\Lambda\Lambda}$. In all fits, the $\omega\Lambda\Lambda$ coupling is kept fixed to $g_{\omega\Lambda\Lambda} = 2g_{\omega NN}/3$. The last column gives the χ^2 by degree of freedom for each fit. Errors are statistical and have been obtained by increasing the value of χ^2 by one unit.

determination of the Λ-core potential do not constitute an important obstacle to learn details about the ΛΛ interaction.

Fits using short distance repulsive Λ-helium core potentials (YNG or SW1) provide significantly higher values of χ^2/dof than those obtained when the ORG or BOY potentials are used for helium. Besides, the only statistically significant contribution to the χ^2/dof comes from the helium datum. From this fact, one might conclude that short distance repulsive potentials for helium are not favored by the experimental value of the ${}^{\;\;6}_{\Lambda\Lambda}$He binding energy. That contradicts the findings of Refs. [22, 29] where it was shown that short distance repulsive Λ-helium potentials were favored by the experimental value of the mesonic decay width of the ${}^{\;\;5}_{\Lambda}$He hypernucleus. However it is difficult to draw any firm conclusion because, as we will see in Subsect. 4.4, YNG and SW1 potentials for helium are not so much statistically disfavored when $r_{12}-$correlations are included in the ΛΛ wave–function. The HE term in Eq. (5), which expected value vanishes for HF-type wave–functions but does not when $r_{12}-$correlations are included, improves the simultaneous description of an extremely light hypernucleus, as helium, and not as light ones, as beryllium or boron.

For the sake of simplicity, when quoting our final HF results, we take for the central value and its statistical error the results obtained with a BOY $\Lambda-$core interaction for all hypernuclei[9]. The results obtained with the rest of the potentials are used to estimate the size of the systematic error due to the Λ-core potential uncertainties. To be more

[9]The $g_{\sigma\Lambda\Lambda}$ values obtained when we use the ORG or BOY Λ-core potentials for helium are practically

specific, for a given value of the cutoff mass $\Lambda_{\sigma\Lambda\Lambda}$ we take for this systematic error the statistical dispersion between the different values of $g_{\sigma\Lambda\Lambda}$ obtained with each of the $\Lambda-$core potentials. Besides we also include another systematic error to account for the dynamical re-ordering effect in the nuclear core due to the presence of the second Λ, as we discussed in Sect. 2 after Eq. (5).

Thus for the results of Table 6 corresponding to $g_{\omega\Lambda\Lambda}/g_{\omega NN}$ =2/3, we find

$$g_{\sigma\Lambda\Lambda}/\sqrt{4\pi} = \left\{ \begin{array}{ll} 3.23 \pm 0.03 \pm 0.02 \pm 0.03 & \Lambda_{\sigma\Lambda\Lambda} = 1 \text{ GeV} \\ 2.37 \pm 0.02 \pm 0.01 \pm 0.02 & \Lambda_{\sigma\Lambda\Lambda} = 2 \text{ GeV} \end{array} \right. \tag{54}$$

where the first error is statistical and the second and third ones are the systematic errors due to our uncertainties in the $\Lambda-$core potential and in our treatment of the dynamics of the nuclear core, respectively. The latter one should account for an uncertainty of about 0.5 MeV, as discussed in Sect. 2, in our theoretical determination of $B_{\Lambda\Lambda}$. For this systematic error we have taken an error of the same size as the statistical one. Thus, the inclusion of this error should account for an uncertainty of about 0.5 MeV (approximate size of the typical errors of the experimental data for $\Delta B_{\Lambda\Lambda}$) in our determination of the total energies of the double$-\Lambda$ hypernuclei. By adding all errors in quadratures, because all of them come from totally uncorrelated sources, we finally obtain

$$g_{\sigma\Lambda\Lambda}/\sqrt{4\pi} = \left\{ \begin{array}{ll} 3.23 \pm 0.05 & \Lambda_{\sigma\Lambda\Lambda} = 1 \text{ GeV} \\ 2.37 \pm 0.03 & \Lambda_{\sigma\Lambda\Lambda} = 2 \text{ GeV} \end{array} \right. \tag{55}$$

As mentioned above, in Ref. [46] the hyperon-nucleon scattering data were fitted with $g_{\omega\Lambda\Lambda}/g_{\omega NN}$ =2/3, $\Lambda_{\sigma\Lambda\Lambda}$ = 1 GeV and $g_{\sigma\Lambda\Lambda}/\sqrt{4\pi}$=2.138. This coupling constant is not directly comparable with that in Eq. (55), because the one determined in this work corresponds to an effective interaction. We will give some more details in the Subsects. 4.5 and 4.7.

The $\Lambda\Lambda$ potential used up to here has some non-localities, namely the terms proportional to

$$\cdots \left[\left(\vec{\nabla} \tilde{\mathbf{Y}}(\alpha, r) \right)_L \cdot \vec{\nabla} + \tilde{\mathbf{Y}}(\alpha, r) \nabla^2 \right] \tag{56}$$

in Eqs. (24) and (25). Because of the small momentum of the Λ particles in the hypernuclei and because these terms are suppressed by powers of $(m_{\text{meson}}/m_{\text{baryon}})^2$, the contribution of these non-localities is small. In order to have a local potential to be plotted, we have dropped out these terms and redone the fits. We find fits of similar quality to those obtained with the non-local $\Lambda\Lambda$ interaction and values of $g_{\sigma\Lambda\Lambda}$ smaller than the previous ones by less than about 0.5%, indicating that the effect of the non-local terms is negligible.

In Fig. 2, we analyze the dependence of the $\Lambda\Lambda$ interaction on the value of the $\omega\Lambda\Lambda$ coupling parameter, $g_{\omega\Lambda\Lambda}$, and the cutoff $\Lambda_{\sigma\Lambda\Lambda}$. We show different local $\Lambda\Lambda$ potentials,

the same, and they only differ by less than one third of the statistical error of any of them. Thus, we have decided to quote those results obtained from a BOY $\Lambda-$helium core interaction in order to be able to use the same $\Lambda-$core potential for all hypernuclei studied in this paper.

obtained from best fits to the data. Despite the different shape and magnitude of the interactions shown in the figure, all of them give values for χ^2/dof of the order of 1, indicating the goodness of the fits and the impossibility of selecting any of them only by means of the binding energies, $B_{\Lambda\Lambda}$. The greater the parameter $g_{\omega\Lambda\Lambda}$, the smaller the statistical and systematic errors in the fitted parameter $g_{\sigma\Lambda\Lambda}$ are. Thus, the systematic (statistical) errors due to the uncertainty in the Λ-core potential vary from 2% (2%) for $g_{\omega\Lambda\Lambda}/g_{\omega NN}$ =1/3, to 0.2% (0.3%) for $g_{\omega\Lambda\Lambda}/g_{\omega NN}$ =4/3. Also the χ^2/dof values decrease moderately for increasing values of the ratio $g_{\omega\Lambda\Lambda}/g_{\omega NN}$.

As can be seen in Fig. 2 for a fixed value of the cutoff $\Lambda_{\sigma\Lambda\Lambda}$, all potentials coincide at the same point. That implies[10] that there is a linear correlation between the couplings $g^2_{\sigma\Lambda\Lambda}$, $\hat{\mathbf{g}}^2_{\omega\Lambda\Lambda}$, defined in Eq. (25), and $(\hat{\mathbf{g}}^2_{\omega\Lambda\Lambda} - g^2_{\omega\Lambda\Lambda})$. Indeed we find excellent fits of the couplings to a dependence of the type

$$g^2_{\sigma\Lambda\Lambda} \;\; = \;\; a + b \times \hat{\mathbf{g}}^2_{\omega\Lambda\Lambda} + c \times (g^2_{\omega\Lambda\Lambda} - \hat{\mathbf{g}}^2_{\omega\Lambda\Lambda}), \tag{57}$$

with approximately similar values for the parameters b and c, and certainly compatible within the statistical errors. Thus, there is an accidental cancelation of the dependence of Eq. (57) on $\hat{\mathbf{g}}^2_{\omega\Lambda\Lambda}$. To take advantage of this fact, we perform a two parameter fit and we find

$$\frac{g^2_{\sigma\Lambda\Lambda}}{4\pi} = \begin{cases} (2.97 \pm 0.19) + (0.830 \pm 0.011) \times \frac{g^2_{\omega\Lambda\Lambda}}{4\pi}, & \chi^2/dof = 0.01, \quad \Lambda_{\sigma\Lambda\Lambda} = 1\,\mathrm{GeV} \\ (1.58 \pm 0.09) + (0.448 \pm 0.005) \times \frac{g^2_{\omega\Lambda\Lambda}}{4\pi}, & \chi^2/dof = 0.02, \quad \Lambda_{\sigma\Lambda\Lambda} = 2\,\mathrm{GeV} \end{cases} \tag{58}$$

for our local family of potentials.

For the the full non-local $\Lambda\Lambda$ potential, we find

$$\frac{g^2_{\sigma\Lambda\Lambda}}{4\pi} = \begin{cases} (3.00 \pm 0.19) + (0.836 \pm 0.011) \times \frac{g^2_{\omega\Lambda\Lambda}}{4\pi}, & \chi^2/dof = 0.02, \quad \Lambda_{\sigma\Lambda\Lambda} = 1\,\mathrm{GeV} \\ (1.58 \pm 0.09) + (0.454 \pm 0.005) \times \frac{g^2_{\omega\Lambda\Lambda}}{4\pi}, & \chi^2/dof = 0.02, \quad \Lambda_{\sigma\Lambda\Lambda} = 2\,\mathrm{GeV} \end{cases} \tag{59}$$

To perform the fits in both the local (Eq. (58)) and non-local (Eq. (59)) cases, we add in quadrature, for each value of $g_{\omega\Lambda\Lambda}$, the statistical and systematic errors of the fitted parameter $g_{\sigma\Lambda\Lambda}$.

We would like also to mention that, here again, as we expected after our discussion in Eq. (28), and in contrast to the findings of Ref. [46], there is a strong correlation between the parameters $g_{\sigma\Lambda\Lambda}$ and $\Lambda_{\sigma\Lambda\Lambda}$ and the quantity $g_{\sigma\Lambda\Lambda} \times (1 - m^2_\sigma/\Lambda^2_{\sigma\Lambda\Lambda})$ remains constant within approximately 3%. This means that, within the HF frame of the analysis of $\Lambda\Lambda$ hypernuclei, the use of different cutoffs $\Lambda_{\sigma\Lambda\Lambda}$ only amounts to redefine the $g_{\sigma\Lambda\Lambda}$ coupling. Then the point at which the potentials coincide is approximately the same for both sets of $\Lambda\Lambda$ potentials ($\Lambda_{\sigma\Lambda\Lambda}$ = 1 GeV and $\Lambda_{\sigma\Lambda\Lambda}$ = 2 GeV), as can be seen in Fig. 2.

[10]Let us suppose that the point where all potentials coincide is r_0 and the common value of the potential is V_0. Then one finds

$$V_0 = V_\sigma^{L=S=0}(r_0) + V_\omega^{L=S=0}(r_0),$$

equation which automatically provides a linear relation between the couplings $g^2_{\sigma\Lambda\Lambda}$, $\hat{\mathbf{g}}^2_{\omega\Lambda\Lambda}$ and $(\hat{\mathbf{g}}^2_{\omega\Lambda\Lambda} - g^2_{\omega\Lambda\Lambda})$.

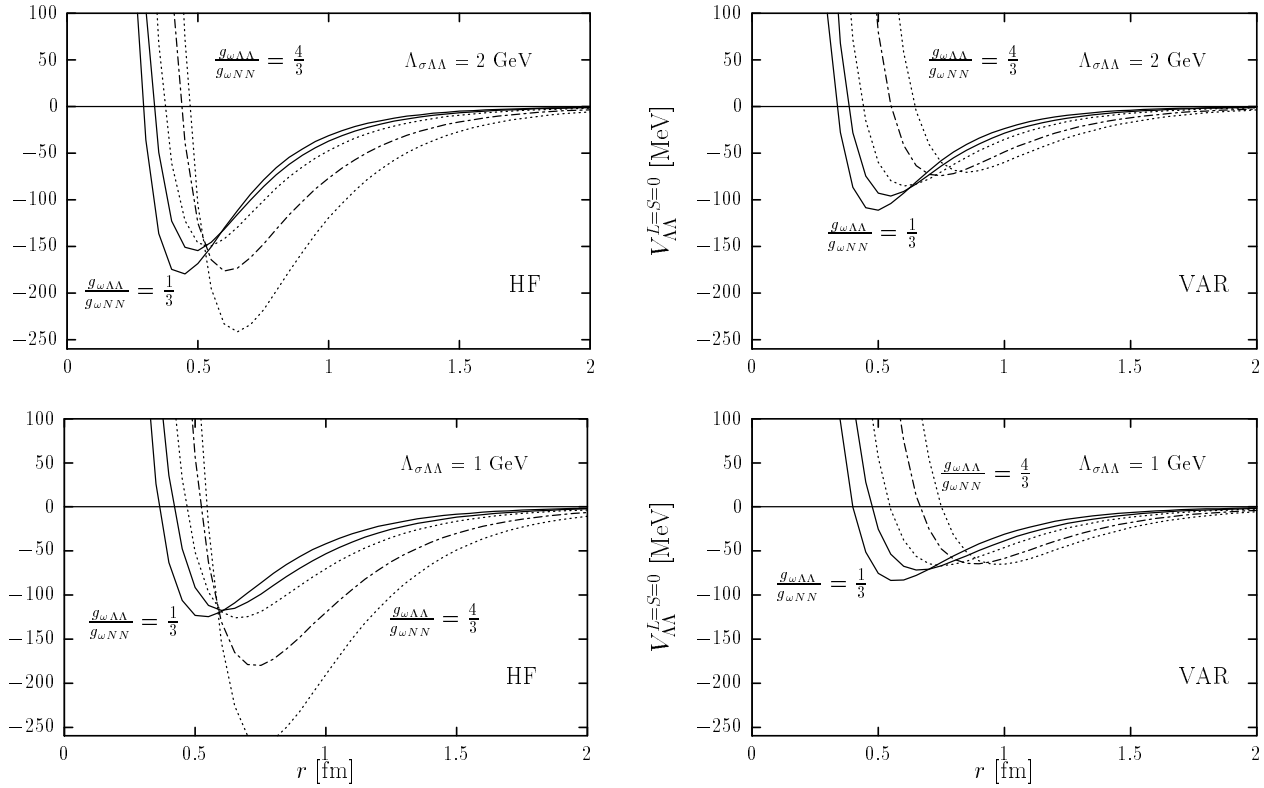

Figure 2: Different $^1S_0$ $\Lambda\Lambda$ potentials, obtained from fits to $B_{\Lambda\Lambda}$. Left (right) figures correspond to results obtained within the HF (VAR) approach. In all figures the five curves correspond to the values 1/3, 1/2, 2/3, 1 and 4/3 for the ratio $g_{\omega\Lambda\Lambda}/g_{\omega NN}$. The cutoff mass $\Lambda_{\sigma\Lambda\Lambda}$ is 2 GeV (top) or 1 GeV (bottom). We have used a local $\Lambda\Lambda$ potential, as described in the text after Eq. (56). BOY Λ-core potentials were used in all cases.

	$\Lambda_{\sigma\Lambda\Lambda} = 1$ GeV		$\Lambda_{\sigma\Lambda\Lambda} = 2$ GeV	
$g_{\omega\Lambda\Lambda}/g_{\omega NN}$	$\frac{g^{\rm pert}_{\sigma\Lambda\Lambda} - g^{\rm HF}_{\sigma\Lambda\Lambda}}{g^{\rm HF}_{\sigma\Lambda\Lambda}}$ (%)	stat$[g^{\rm HF}_{\sigma\Lambda\Lambda}]$ (%)	$\frac{g^{\rm pert}_{\sigma\Lambda\Lambda} - g^{\rm HF}_{\sigma\Lambda\Lambda}}{g^{\rm HF}_{\sigma\Lambda\Lambda}}$ (%)	stat$[g^{\rm HF}_{\sigma\Lambda\Lambda}]$ (%)
1/3	5.2	1.8	5.9	1.8
1/2	3.2	1.2	3.7	1.2
2/3	1.9	0.9	2.5	0.8
1	0.7	0.5	1.0	0.5
4/3	0.3	0.3	0.4	0.3

Table 7: Comparison of perturbative (pert) and HF results for different types of $\Lambda\Lambda$ interaction (the small non-local terms have been neglected). BOY Λ-core potentials have been used for all hypernuclei. The columns labelled by stat$[g^{\rm HF}_{\sigma\Lambda\Lambda}]$ stands for the statistical error (in percentage) of the fitted parameter $g^{\rm HF}_{\sigma\Lambda\Lambda}$.

4.3 A Perturbative Approach

The fact that the quantity $\Delta B_{\Lambda\Lambda}/2B_{\Lambda\Lambda}$ is smaller than one for all hypernuclei considered in this work has made us to explore the possibility of using a perturbative scheme. Surprisingly, we find that in a good approximation the $\Lambda\Lambda$ potential, $V_{\Lambda\Lambda}$, can be treated perturbatively, as the results of Table 7 indicate. In this table, we compare the HF-local results of Eq. (58) with those obtained from best fits to the data using the approximation

$$\Delta B_{\Lambda\Lambda} = -\left\langle V_{\Lambda\Lambda}(\vec{r_1} - \vec{r_2}) - \frac{\vec{\nabla}_1 \cdot \vec{\nabla}_2}{M_A} \right\rangle_{\mathbf{\Phi^{(0)}_{\Lambda\Lambda}}} , \tag{60}$$

where $\langle \mathcal{O} \rangle_\Phi$ denotes the expected value of the operator $\mathcal{O}$ in the state Φ and $\mathbf{\Phi^{(0)}_{\Lambda\Lambda}} = \varphi_{\mathbf{\Lambda}}(\vec{\mathbf{r_1}}) \cdot \varphi_{\mathbf{\Lambda}}(\vec{\mathbf{r_2}})$, where φ_Λ is the Λ-wave function in the single–Λ hypernucleus ${}^{A+1}_{\Lambda}Z$. To simplify we have also neglected the non-local terms in $V_{\Lambda\Lambda}$. Note also that the expected value of the HE term is zero in the state $\mathbf{\Phi^{(0)}_{\Lambda\Lambda}}$.

In the worst of the cases ($g_{\omega\Lambda\Lambda}/g_{\omega NN} = 1/3$ and $\Lambda_{\sigma\Lambda\Lambda} = 2$ GeV) the ratio $\frac{g^{\rm pert}_{\sigma\Lambda\Lambda} - g^{\rm HF}_{\sigma\Lambda\Lambda}}{g^{\rm HF}_{\sigma\Lambda\Lambda}}$, which accounts for the difference between the HF and the perturbative approaches, is only 5.9% and its value decreases to only 0.3% for the case $g_{\omega\Lambda\Lambda}/g_{\omega NN} = 4/3$, being this latter value of the same order as the the statistical error (in percentage) of the fitted parameter $g^{\rm HF}_{\sigma\Lambda\Lambda}$. Perturbative values of the fitted parameter $g_{\sigma\Lambda\Lambda}$ are always larger than the HF ones, though for most of the cases both sets of couplings are compatible within total (statistical and systematic) errors. The values of χ^2/dof are about a factor of 1.5 larger within the perturbative approximation than in the HF one.

The fact that the perturbative and the HF schemes give the same results within approximately 5% can be used to understand the existence of strong linear correlations of the type of Eq. (57). For simplicity let us discuss only the case of the local $\Lambda\Lambda$ potential. For each hypernucleus (helium, beryllium and boron), because Eq. (60) is satisfied in

a good approximation, one gets a linear relation between the couplings $g^2_{\sigma\Lambda\Lambda}$, $g^2_{\omega\Lambda\Lambda}$ and $\hat{\mathbf{g}}^2_{\omega\Lambda\Lambda}$, namely

$$\begin{aligned} g^2_{\sigma\Lambda\Lambda} &\approx \frac{-\Delta B_{\Lambda\Lambda}}{\langle V^{L=S=0}_{L\sigma}/g^2_{\sigma\Lambda\Lambda}\rangle_{\mathbf{\Phi^{(0)}_{\Lambda\Lambda}}}} - \frac{\langle V^1_\omega\rangle_{\mathbf{\Phi^{(0)}_{\Lambda\Lambda}}}}{\langle V^{L=S=0}_{L\sigma}/g^2_{\sigma\Lambda\Lambda}\rangle_{\mathbf{\Phi^{(0)}_{\Lambda\Lambda}}}} \times \hat{\mathbf{g}}^2_{\omega\Lambda\Lambda} \\ &- \frac{\langle V^2_\omega\rangle_{\mathbf{\Phi^{(0)}_{\Lambda\Lambda}}}}{\langle V^{L=S=0}_{L\sigma}/g^2_{\sigma\Lambda\Lambda}\rangle_{\mathbf{\Phi^{(0)}_{\Lambda\Lambda}}}} \times (g^2_{\omega\Lambda\Lambda} - \hat{\mathbf{g}}^2_{\omega\Lambda\Lambda}), \end{aligned} \tag{61}$$

where

$$V^1_\omega(r) = \frac{m_\omega}{4\pi}\tilde{\mathbf{Y}}(\omega, r), \tag{62}$$

$$V^2_\omega(r) = \left[V^{L=S=0}_{L\omega}(r) - \hat{\mathbf{g}}^2_{\omega\Lambda\Lambda}V^1_\omega(r)\right]/(g^2_{\omega\Lambda\Lambda} - \hat{\mathbf{g}}^2_{\omega\Lambda\Lambda}), \tag{63}$$

and $V^{L=S=0}_{L\alpha}(\alpha = \sigma, \omega)$ is the local part of $V^{L=S=0}_\alpha$. The fact that we find a reasonable simultaneous description of the three hypernuclei, with the same value of the parameter $g_{\sigma\Lambda\Lambda}$ for each value of $g_{\omega\Lambda\Lambda}$, implies that the coefficients of the couplings in Eq. (61) are rather independent of the nuclear core.

Note that in the case of the non-local potential, linear relations between the couplings can be also obtained once the non-local terms of the $\Lambda\Lambda$ potential are included in the right hand side of Eq. (61).

4.4 $\Lambda\Lambda$ Interaction: Variational Results

In Table 8, for given values of the ratio $g_{\omega\Lambda\Lambda}/g_{\omega NN}$ and of the cutoff $\Lambda_{\sigma\Lambda\Lambda}$, we show the values of the parameter $g_{\sigma\Lambda\Lambda}$ obtained from best fits to the $B_{\Lambda\Lambda}$ binding energies by using the variational method described in Subsect. 2. We use the same procedure to give the central values and the statistical and systematic errors as in the HF case. In all situations (i.e., different ratios $g_{\omega\Lambda\Lambda}/g_{\omega NN}$, different values for the cut-off parameter $\Lambda_{\sigma\Lambda\Lambda}$ and Λ-core potentials), we find statistically acceptable fits. We would like just to mention that the use of the ORG potential for helium provides smaller χ^2/dof than the BOY Λ-core potential used to quote the central value of the fitted parameter. Namely, values of χ^2/dof smaller than 0.1 for the ORG potential versus values around 0.5 for the BOY case. The HE term improves significantly the simultaneous description of all three hypernuclei when Λ-core potentials (BOY,YNG, SW1 or SW2) not as attractive at short distances as the ORG one are used for helium. To be more specific, for the case of the BOY (YNG) potential, if the HE term is not included the typical values for χ^2/dof are of the order of 1.5 (4.0), between two or three times larger than those obtained when the HE piece is considered. In all cases the largest contribution to the χ^2/dof comes from the helium piece of data.

Local and non-local potentials lead to different values for the fitted coupling $g_{\sigma\Lambda\Lambda}$. These changes vary from 1% to 7% when the ratio $g_{\omega\Lambda\Lambda}/g_{\omega NN}$ increases and they are significantly greater than the statistical errors (except for the lowest value of $g_{\omega\Lambda\Lambda}$) and

		$g_{\sigma\Lambda\Lambda}/\sqrt{4\pi}$	
$g_{\omega\Lambda\Lambda}/g_{\omega NN}$	$\Lambda_{\sigma\Lambda\Lambda}$ (GeV)	LOCAL	NON-LOCAL
1/3	1	$1.89 \pm 0.03 \pm 0.02$	$1.91 \pm 0.03 \pm 0.02$
1/2	1	$2.33 \pm 0.03 \pm 0.02$	$2.38 \pm 0.03 \pm 0.02$
2/3	1	$2.76 \pm 0.03 \pm 0.02$	$2.85 \pm 0.03 \pm 0.02$
1	1	$3.55 \pm 0.03 \pm 0.02$	$3.74 \pm 0.03 \pm 0.02$
4/3	1	$4.26 \pm 0.03 \pm 0.02$	$4.56 \pm 0.03 \pm 0.02$
1/3	2	$1.397 \pm 0.018 \pm 0.008$	$1.415 \pm 0.018 \pm 0.008$
1/2	2	$1.764 \pm 0.017 \pm 0.007$	$1.796 \pm 0.016 \pm 0.007$
2/3	2	$2.145 \pm 0.016 \pm 0.007$	$2.199 \pm 0.016 \pm 0.006$
1	2	$2.876 \pm 0.017 \pm 0.006$	$3.005 \pm 0.017 \pm 0.006$
4/3	2	$3.551 \pm 0.019 \pm 0.006$	$3.772 \pm 0.018 \pm 0.006$

Table 8: VAR results for $g_{\sigma\Lambda\Lambda}$ obtained from best fits to the $B_{\Lambda\Lambda}$ data. The several rows correspond to different values for the ratio $g_{\omega\Lambda\Lambda}/g_{\omega NN}$ and different values of the cutoff $\Lambda_{\sigma\Lambda\Lambda}$. Central values and their statistical uncertainties (first set of errors) are obtained using BOY Λ-core potentials for all hypernuclei. The χ^2/dof values for all cases are about 0.4-0.5. Statistical errors are obtained by increasing the value of χ^2 by one unit. The second set of errors account for the dispersion in the results due to the use of different Λ-core potentials, as it was discussed in Subsect. 4.2. To account for dynamical re-ordering effects in the nuclear core due to the presence of the second Λ, further systematic errors should be added. As it was discussed in Subsect. 4.2, the statistical errors provide a reasonable estimate of these additional systematic errors. We give results for the full $\Lambda\Lambda$ interaction (non-local) and the local reduction of it discussed in the text after Eq. (56).

much more appreciable than those found within the HF scheme. Variations of the cutoff mass $\Lambda_{\sigma\Lambda\Lambda}$ lead to changes in the quantity $g_{\sigma\Lambda\Lambda} \times (1 - m_\sigma^2/\Lambda_{\sigma\Lambda\Lambda}^2)$ from 3% to 10% when the ratio $g_{\omega\Lambda\Lambda}/g_{\omega NN}$ increases from 1/3 to 4/3. These changes are again much more pronounced here than in the HF case, indicating that the variational wave functions for the two Λ's system lead to bigger values of the transfered momentum between both particles. This is also consistent with the fact, mentioned above, that within the VAR scheme non-local and local potentials lead to differences much more significant than in the HF one.

In Fig. 2 (right) we show the local $\Lambda\Lambda$ potentials corresponding to the different combinations of the ratio $g_{\omega\Lambda\Lambda}/g_{\omega NN}$ and the cutoff mass parameter $\Lambda_{\sigma\Lambda\Lambda}$ given in Table 8. In this figure, for comparison, and in the same scale, the HF local potentials discussed in the previous section are also shown. VAR potentials are significantly less attractive than HF ones, as the variational principle ensures. The larger the ratio $g_{\omega\Lambda\Lambda}/g_{\omega NN}$, the bigger this effect is.

For both local and non-local VAR potentials, we find that the coupling constants are correlated in the form given in Eq. (57), but with poorer χ^2/dof values (with χ^2/dof ranging from 0.12, for a local $\Lambda\Lambda$ interaction and $\Lambda_{\sigma\Lambda\Lambda} = 1$ GeV, to 0.8, for a local $\Lambda\Lambda$ interaction and $\Lambda_{\sigma\Lambda\Lambda} = 2$ GeV) than in the HF case. But, for this variational scenario, the values of parameters b and c of Eq. (57) are not similar, and a linear relationship between $g_{\sigma\Lambda\Lambda}^2$ and $g_{\omega\Lambda\Lambda}^2$ can not be casted. Therefore, unlike the HF families, the obtained families of variational potentials do not coincide at a single point[11].

The existence of a relation of the type of Eq. (57) also in the VAR scheme can be understood if one applies the same type of considerations used in the discussion of Eqs.(60) – (61) to the relation

$$B_{\Lambda\Lambda} = -\left\langle \sum_{i=1,2} \left(-\frac{\vec{\nabla}_i^2}{2\mu_A} + \mathcal{V}_{\Lambda A}(\vec{r_i}) \right) + V_{\Lambda\Lambda}(\vec{r_1} - \vec{r_2}) - \frac{\vec{\nabla}_1 \cdot \vec{\nabla}_2}{M_A} \right\rangle_{\mathbf{\Phi_{\Lambda\Lambda}^{VAR}}} . \tag{64}$$

In Fig. 3 we show graphically the differences between the fitted parameter $g_{\sigma\Lambda\Lambda}$ obtained in the HF and VAR schemes for different values of $g_{\omega\Lambda\Lambda}$, different cutoffs $\Lambda_{\sigma\Lambda\Lambda}$ and using local (dotted lines) and non-local (solid lines) $\Lambda\Lambda$ interactions. The non-local part of the $\Lambda\Lambda$ potential is repulsive, as can be deduced from the figure. However, the differences between VAR local and non-local parameters are always much smaller than the differences between HF and VAR parameters.

Once we have seen that within the HF approach (or even in the perturbative approximation) we could described reasonably well the experimental data, one might question about the need of performing a variational study of the double$-\Lambda$ hypernuclei. To check this in Table 9 we compare, for a fixed $\Lambda\Lambda$ interaction, the results of the perturbative, HF

[11] The equation $dV_{\Lambda\Lambda}(r)/dg_{\omega\Lambda\Lambda} = 0$ has as solution a value of r independent of $g_{\omega\Lambda\Lambda}$ (what implies that all potentials coincide in a single point) only if there exist a linear relation between the couplings $g_{\sigma\Lambda\Lambda}^2$ and $g_{\omega\Lambda\Lambda}^2$ and a small term proportional to $(m_\omega/m_\Lambda)^2 g_{\omega\Lambda\Lambda} f_{\omega\Lambda\Lambda}$, in the $\omega-$exchange part of the potential is neglected.

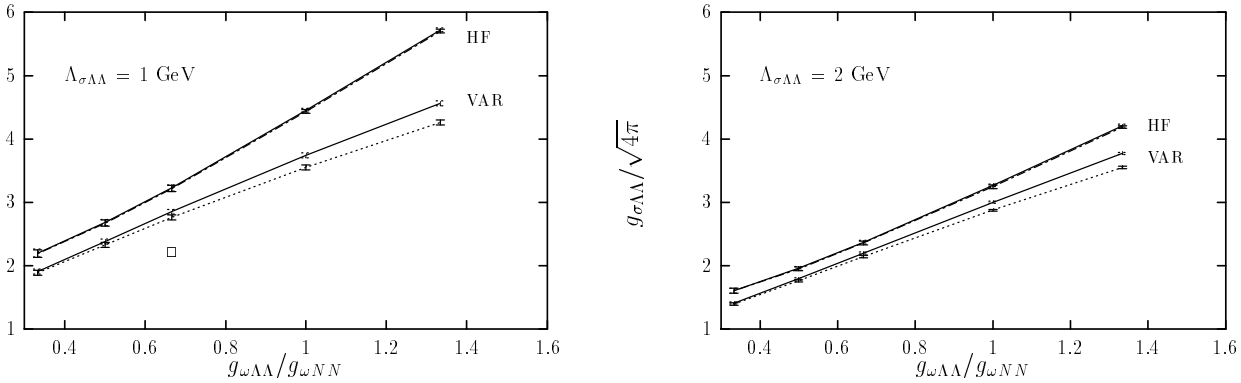

Figure 3: Different couplings $g_{\sigma\Lambda\Lambda}/\sqrt{4\pi}$ versus $g_{\omega\Lambda\Lambda}/g_{\omega NN}$ found for the ${}^1S_0$ $\Lambda\Lambda$ potentials obtained from best fits to $B_{\Lambda\Lambda}$ data within the HF and VAR approaches. The cutoff mass $\Lambda_{\sigma\Lambda\Lambda}$ is 1 GeV (left) or 2 GeV (right). In both plots the solid (dotted) lines correspond to a non-local (local, as described in the text after Eq. (56)) $\Lambda\Lambda$ interaction and the five points with errors correspond to the values 1/3, 1/2, 2/3, 1 and 4/3 for the ratio $g_{\omega\Lambda\Lambda}/g_{\omega NN}$. The lines have been drawn only for guiding the eye. BOY Λ-core potentials were used in all cases. For comparison, the square in the left figure stands for the potential of model $\hat{A}$ of Ref. [46].

and VAR approaches for the binding energy of ${}^{13}_{\Lambda\Lambda}$B. We also show the result obtained if no correlations (i.e., dependence on r_{12}) are included in the variational wave function (that corresponds to fix $c = 0$ in the variational basis of Eq.(10)). Even in this latter case the VAR scheme does not reduce to the HF one because the wave function can not be gathered as a product of a function of r_1 times the same function now of r_2. The HF approach can be considered as a variational one, where the space of functions are limited to those which can be written in a factorizable way. The numbers of the table show that enlarging this space to include some non-factorizable wave–functions (but without dependence on r_{12} yet) does not modify drastically the HF results. However, the inclusion of $r_{12}-$correlations has a drastic effect in the binding energy. This can be also appreciated in Fig. 4, where the dependence on r_{12} of the $\Lambda\Lambda$ potential (used to obtain the numbers of Table 9) and the HF and VAR densities of probability of finding the two Λ's at a relative distance r_{12} ($\mathbf{P}(r_{12})$, defined in Eq. (7)) are shown. The effect of the inclusion of $r_{12}-$correlations is twofold. First, it reduces the probability of finding the two particles at very short distances, where the potential is highly repulsive, with values at $r_{12} = 0$ as large as tens of thousands of MeV. Second, it increases the probability of finding the particles at relative distances of the order of 1 fm, where the potentials have their maximum attraction. Thus, as a net effect an important reduction of the expected value of the energy of the system is provided.

The $\Lambda\Lambda$ interactions obtained by $\sigma - \omega$ exchange behave almost like a hard-core at short distances, then in a very small region and close to the origin ($r_{12} \approx 0.5$ fm), they pass from being extremely repulsive to reach their maximum attraction. On the other hand, note that due to the phase space $\mathbf{P}(r_{12})$ is suppressed at small values of r_{12} by at least a factor r_{12}^2. Thus the HF two body probability $\mathbf{P}(r_{12})$ takes very small values in the region where the potential is repulsive but it also misses the maximum attraction

	$B_{\Lambda\Lambda}$ [$^{13}_{\Lambda\Lambda}$B] [MeV]
PERT.	27.3
HF	27.8
VAR NO CORR.	28.4
VAR	36.9

Table 9: Comparison of the results obtained for $B_{\Lambda\Lambda}$ in boron double$-\Lambda$ hypernuclei, using different approximations. In all cases the same local $\Lambda\Lambda$ interaction (with parameters $g_{\sigma\Lambda\Lambda}/\sqrt{4\pi}$, $g_{\omega\Lambda\Lambda}/g_{\omega NN}$ and $\Lambda_{\sigma\Lambda\Lambda}$ fixed to 3.22, 2/3 and 1 GeV respectively) and BOY Λ-core potential were used. The coupling $g_{\sigma\Lambda\Lambda}$ was obtained from a best fit to the data within the HF approach (see results of Eq. (58)). The first, second and fourth rows correspond to the standard perturbative, HF and VAR calculations. The third (labeled VAR NO CORR.) row corresponds to a variational calculation where the ansatz wave function does not depend on r_{12} (that corresponds to fix $c = 0$ in the variational basis of Eq.(10)). The experimental binding energy for boron double$-\Lambda$ hypernuclei is 27.5 ± 0.7 MeV.

l	0	1	2	3	4	5	6
$\mathcal{P}_l$	0.9727	0.02280	0.00200	0.00075	0.00054	0.00040	0.00028
$\sum_{k=0}^{l} \mathcal{P}_k$	0.9727	0.9955	0.9975	0.9982	0.9988	0.9991	0.9994

Table 10: Probabilities $\mathcal{P}_l$ (defined in Eq. (12)) for several waves. Results were obtained for boron double$-\Lambda$ hypernucleus. A local $\Lambda\Lambda$ interaction (with parameters $g_{\sigma\Lambda\Lambda}/\sqrt{4\pi} = 2.76$, $g_{\omega\Lambda\Lambda}/g_{\omega NN} = 2/3$ and $\Lambda_{\sigma\Lambda\Lambda} = 1$ GeV, see Table 8) and BOY Λ-core potentials were used. The errors are always less than one unit in the last digit.

region of the $\Lambda\Lambda$ interaction. The inclusion of a dependence on r_{12} in the variational wave function allows both to keep small (and even smaller than in the HF case) the two body probability in the hard-core region and to increase this two body probability in the adjacent region where the potential reaches its maximum attraction. The steeper $\Lambda\Lambda$ potential, the bigger the difference between the VAR and HF predictions becomes. Thus, the effects of including $r_{12}-$correlations are much more pronounced for values of the ratio $g_{\omega\Lambda\Lambda}/g_{\omega NN}$ bigger than the standard 2/3 one used in this discussion. Therefore, the VAR approach, including correlations, provides the same binding energies than the HF approach with significantly less attractive $\Lambda\Lambda$ interactions, as we showed in Figs. 2 and 3.

To finish this section we would like to devote a few words to the multipolar content of the VAR wave functions. In Table 10 we show the probability $\mathcal{P}_l$, defined in Eq. (12), of finding each of the two Λ's with angular momentum l and coupled to $L = 0$ for boron. Although a particular $\Lambda\Lambda$ interaction is used, the gross features of the multipolar decomposition do not depend significantly on the selected interaction. Only few multipoles

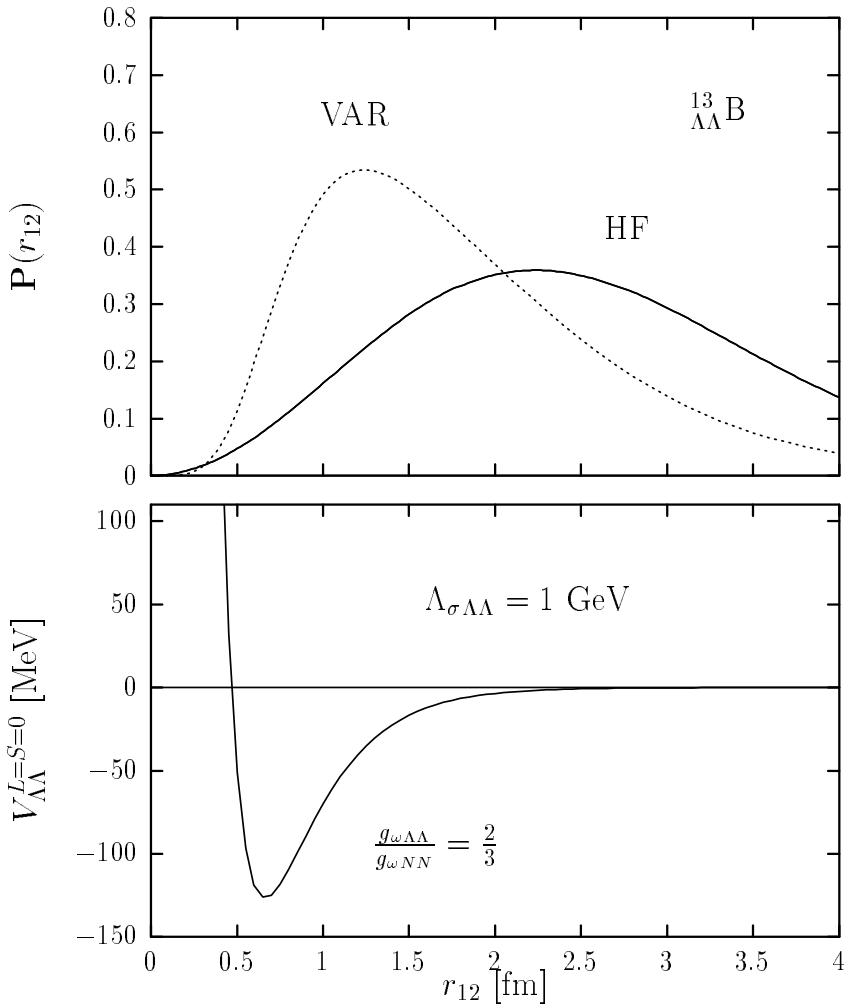

Figure 4: Top: HF (solid) and VAR (dotted) probabilities of finding the two Λ's at a relative distance r_{12} as a function of this distance. Computations were done in $^{13}_{\Lambda\Lambda}$B and using the ΛΛ interaction (bottom figure) specified in Table 9.

	$\Lambda_{\phi\Lambda\Lambda}$[GeV]	$g_{\sigma\Lambda\Lambda}/\sqrt{4\pi}$ ($\Lambda_{\sigma\Lambda\Lambda}=1$ GeV) HF	VAR	$g_{\sigma\Lambda\Lambda}/\sqrt{4\pi}$ ($\Lambda_{\sigma\Lambda\Lambda}=2$ GeV) HF	VAR
without ϕ	–	3.23 ± 0.03	2.85 ± 0.03	2.37 ± 0.02	2.199 ± 0.016
with ϕ	1.5	3.38 ± 0.03	2.85 ± 0.03	2.48 ± 0.02	2.232 ± 0.018
	2.0	3.52 ± 0.03	2.74 ± 0.03	2.58 ± 0.02	2.16 ± 0.02
	2.5	3.60 ± 0.03	2.62 ± 0.03	2.64 ± 0.02	2.06 ± 0.02

Table 11: Best fit results for the $\sigma\Lambda\Lambda$-coupling obtained from different non-local $\Lambda\Lambda-$interactions for both HF and VAR approximations. We compare results for both $\sigma+\omega$ (already presented in Tabs. 6 and 8) and $\sigma+\omega+\phi-$interactions. BOY Λ-core potentials were used for the three double$-\Lambda$ hypernuclei. The parameter $g_{\omega\Lambda\Lambda}/g_{\omega NN}$ has been fixed to 2/3. Furthermore, the $\phi-$ couplings have been fixed, by means of $SU(6)$-symmetry, (see Eq. (65)). Errors are only statistical.

contribute[12], being $l=0$ the dominant one and contributing appreciably only up to the waves $l=2$ or $l=3$. The higher the orbital angular momentum of each Λ, the farer from the origin the corresponding wave function is and therefore the smaller the overlap of the two-body wave function with the attractive part of the potential is.

Results of Table 10, which show predominance of the $l=0$ component in the VAR wave–function, do not contradict the fact that correlations are important to lower the energy of the double$-\Lambda$ hypernuclei. Indeed, the hamiltonian is not diagonal in the basis with well defined single–particle orbital angular momentum. Hence, non-diagonal matrix elements contribute significantly to the hamiltonian expectation value.

4.5 Contribution of the $\phi-$Exchange.

In this Subsection we discuss qualitatively the effect of the $\phi-$exchange in the $\Lambda\Lambda$ potential in the medium. The $\phi-$potential can be obtained from that of the $\omega-$exchange given in Eqs (25) – (27) by the obvious substitutions: $m_\omega \to m_\phi$, and $[g,f,\Lambda]_{\omega\Lambda\Lambda} \to [g,f,\Lambda]_{\phi\Lambda\Lambda}$. In the spirit of the Bonn-Jülich models we use $SU(6)$ symmetry to fix the $\phi-$couplings,

$$\begin{aligned} g_{\phi\Lambda\Lambda} &= -g_{\omega\Lambda\Lambda}/\sqrt{2} \\ f_{\phi\Lambda\Lambda} &= \sqrt{2} f_{\omega\Lambda\Lambda}. \end{aligned} \tag{65}$$

As it was discussed in Subsect. 2.1 because within this model the ϕ meson does not couple to nucleons, we do not have much information about the cutoff-mass $\Lambda_{\phi\Lambda\Lambda}$. Assuming that this cutoff should be similar to that entering in the $\omega\Lambda\Lambda-$coupling and certainly

[12]Note that we show probabilities: the components of the wave function for each value of l are given, up to a sign, by the squared root of the numbers presented in the table.

bigger than the ϕ meson mass, we have studied three different values, 1.5, 2 and 2.5 GeV. Results are presented in Tables 11 and 12. We would like to make a few remarks,

- The effect of the $\phi-$exchange depends strongly on the value of the cutoff mass $\Lambda_{\phi\Lambda\Lambda}$, such that this effect passes from being small ($\Lambda_{\phi\Lambda\Lambda} = 1.5$ GeV) to be significant ($\Lambda_{\phi\Lambda\Lambda} = 2.5$ GeV). Indeed, this is easily understood by looking at the top graph of Fig. 5 where the ω and the three $\omega + \phi$ potentials considered in Table 11 are plotted (neglecting the small non-local pieces). The several $\omega + \phi$ potentials significantly differ in the region of relative $\Lambda\Lambda$ distances ranging from 0.1 to 1.3 fm, where the product of the $\Lambda\Lambda$-interaction times the probability ($\mathbf{P}(r_{12})$) of finding the two Λ particles at relative distance r_{12} takes non negligible values.

  As the numbers of Table 12 indicate, the $\phi-$contribution is smaller than the ω meson one and at maximum it might be of the order of 20% of the latter one. This is not surprising, because as we mentioned earlier, the exchange of heavier mesons than the σ and ω ones, essentially modify the short range behavior of the interaction, and hence becomes more significant for processes where larger momentum transfers than those involved here are relevant. On the other hand, by the use of different values of the $\sigma-$cutoff and also different values of $g_{\omega\Lambda\Lambda}$ we have already explored a wide range of short distance behaviors of the effective $\Lambda\Lambda-$interaction in the medium. The above discussion, together with the very scarce set of data available, have prevented us to include the $\phi-$meson contribution in the present determination of the effective $\Lambda\Lambda$ interaction. Its inclusion would require, even assuming $SU(6)-$symmetry, to deal with at least one more free parameter, and it might obscure the analysis presented in this work (differences between HF, perturbative and VAR approaches, size of systematic errors $\cdots$). On the other hand, the possible effect of the $\phi-$exchange potential in the tail of $\Lambda\Lambda$ wave–function, though small, is mostly reabsorbed by the use of effective $\sigma + \omega-$couplings and thus, the inclusion of the ϕ contribution in the potential would not modify significantly the mesonic decay of the double$-\Lambda$ hypernuclei studied in the next Subsection. However, when trying to simultaneously analyze the double$-\Lambda$ hypernuclei data and the $S = -2$ baryon dynamics in the free space, one should not neglect this contribution because it might lead to sizeable changes in the values of the $\sigma-$coupling, as the numbers presented in Table 11 clearly show.

- A distinctive feature of the results presented in Tables 11 and 12, is that the character of the $\phi-$ contribution though attractive within the VAR scheme, is repulsive within the HF one. Hence, the differences between the HF and VAR approaches get amplified. $\phi-$exchange does not lead to a purely repulsive potential, as it is the case for the $\omega-$ meson, because the ratio f/g is positive, instead of negative, and bigger (in absolute value) for the $\phi-$potential than for the $\omega-$ one. Thus, the $\phi-$ potential though much more repulsive than the $\omega-$ one at short distances, becomes however attractive at distances bigger than let us say 0.4 fm (see Fig. 5 [13]). In the case of the HF approach, though the probability $\mathbf{P}(r_{12})$ is quite small at short distances,

[13] Note that in the limit $\Lambda_{\phi\Lambda\Lambda} \to \infty$, the repulsive core becomes a δ peak at the origin.

	$\left\langle V_\phi^L \right\rangle_{\mathbf{\Phi}_{\mathbf{\Lambda\Lambda}}^{(\sigma+\omega)}}$ [MeV]	
$\Lambda_{\phi\Lambda\Lambda}$[GeV]	HF	VAR
1.5	1.95	−0.002
2.0	3.68	−1.14
2.5	4.53	−2.33

Table 12: Expected values of the local part of the $\phi-$potential, for several $\phi\Lambda\Lambda$ cutoffs, in the $\Lambda\Lambda$ state corresponding to the HF and VAR solutions (with no ϕ contribution and $\Lambda_{\sigma\Lambda\Lambda} = 1$ GeV) given in the first row of Table 11. $\phi-$ couplings have been fixed by means of $SU(6)$-symmetry. For comparison, the expected values of $\left\langle V_\omega^L \right\rangle_{\mathbf{\Phi}_{\mathbf{\Lambda\Lambda}}^{(\sigma+\omega)}}$ are 14.68 and 10.02 MeV for the HF and VAR wave–functions respectively.

because the huge and repulsive values taken by the $\phi-$potential close to zero, the balance between the repulsive and attractive contributions favors the former ones. The inclusion of $r_{12}-$correlations in the VAR scheme allows to have simultaneously smaller and bigger values of $\mathbf{P}(r_{12})$ than in the HF case in the regions where the $\phi-$potential is repulsive and attractive respectively. As a net effect, the balance between the repulsive and attractive contributions favors now the latter ones. This is easy to appreciate in Fig. 5.

4.6 Mesonic Decay and Binding Energies of Double−Λ Hypernuclei

One might think that the mesonic decay of these double−Λ hypernuclei could depend significantly on the details of the effective ΛΛ interaction and thus it could be used to differentiate between the different potentials shown in Fig. 2. There are some theoretical uncertainties[14] in the calculation of the mesonic decay of ${}^{5}_{\Lambda}$He [22, 29, 41], related to the nuclear core–Λ interaction, and this has prevented us from looking at ${}^{6}_{\Lambda\Lambda}$He to check the dependence of the mesonic decay on the details of the ΛΛ interaction[15]. Thus, we have looked at the case of ${}^{13}_{\Lambda\Lambda}$B. For this hypernucleus, we find that the pionic decay width of ${}^{12}_{\Lambda}$B changes only around a 5% when different Λ-core potentials (BOY, SW1, SW2) are considered.

The mesonic decay has been computed following the method exposed in Sect 3. We use the ten VAR non-local potentials presented in Table 8, and we find that the mesonic

[14] As can be seen in Fig. 1 and in Table 5, different Λ-core potentials for helium lead to significantly different mean squared radius of the Λ orbiting around the nuclear core. The mesonic decay process is quite sensitive to the tail of the Λ wave–function and then it depends strongly on the details of the Λ-core potential used.

[15] In Refs. [22] and [39] the mesonic decay of the double−Λ hypernucleus ${}^{6}_{\Lambda\Lambda}$He has been calculated.

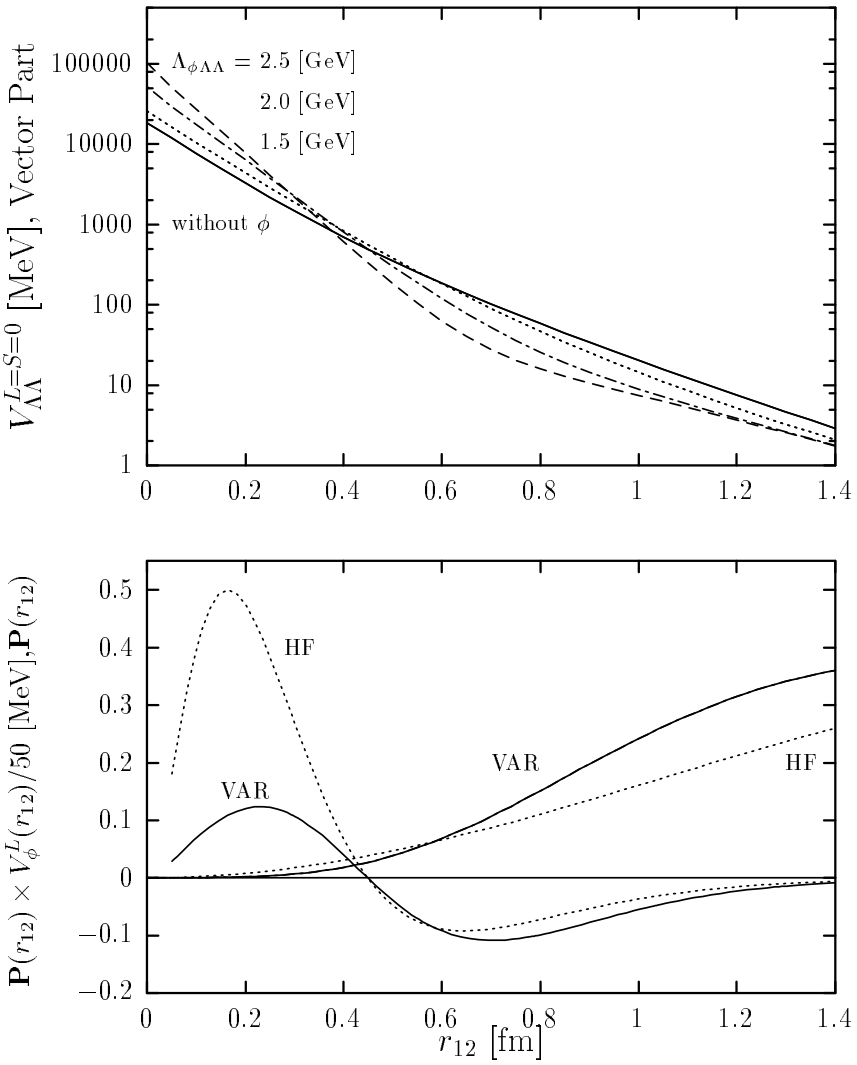

Figure 5: Top: $\omega-$ (solid line) and $\omega+\phi-$ local pieces of the $\Lambda\Lambda$ potentials predicted by $SU(6)$-symmetry. Three different values (1.5, 2.0 and 2.5 GeV) for the cutoff $\Lambda_{\phi\Lambda\Lambda}$ have been used. The larger the $\phi\Lambda\Lambda$ cutoff, the bigger is the resulting repulsion at the origin. Bottom: Two different set of curves are being plotted as a function of the $\Lambda\Lambda$ relative distance, r_{12} : a) HF and VAR probabilities, obtained from the potentials specified in the first row ("without ϕ" and $\Lambda_{\sigma\Lambda\Lambda} = 1$ GeV) of Table 11, of finding the two Λ's at a relative distance r_{12} , b) the product of these probabilities times the $\Lambda_{\phi\Lambda\Lambda} = 2.0$ GeV local $\phi-$potential used in Table 12. This latter set of curves have been divided by a factor 50 and the area below these curves gives, up to a factor 50, the expected values given also in Table 12.

decay width varies by 5% at most, making then this quantity unappropriated to choose between the different potentials discussed above. However, this fact allows us to predict the mesonic decay and, by using the potential of Eq. (47) in addition to Cohen–Kurath spectroscopic factors for the $1p-$shell to describe the ^{11}B, ^{12}C* and ^{12}B* nuclear cores, we find

$$\frac{\Gamma(^{13}_{\Lambda\Lambda}\mathrm{B} \to X + \Lambda + \pi^0)}{\Gamma_\Lambda} = 0.062 \pm 0.002 \pm 0.002, \quad (66)$$

$$\frac{\Gamma(^{13}_{\Lambda\Lambda}\mathrm{B} \to X + \Lambda + \pi^-)}{\Gamma_\Lambda} = 0.270 \pm 0.008 \pm 0.008, \quad (67)$$

where $\Gamma_\Lambda = \Gamma^{(p)}_{free} + \Gamma^{(n)}_{free}$ is the total decay width of the Λ in the vacuum, with $\Gamma^{(\alpha)}_{free}$ defined in Eq. (42). The central values are obtained with $g_{\omega\Lambda\Lambda}/g_{\omega NN} = 2/3$ and $\Lambda_{\sigma\Lambda\Lambda} = 1$ GeV. The first set of errors accounts for the statistical error of $g_{\sigma\Lambda\Lambda}$ whereas the second one accounts for the spreading of the results obtained with the different combinations of ratios $g_{\omega\Lambda\Lambda}/g_{\omega NN}$ (1/3, 1/2, 2/3, 1, 4/3) and values (1 and 2 GeV) for the cutoff $\Lambda_{\sigma\Lambda\Lambda}$.

Further systematic errors should be added to those quoted in Eqs. (66) – (67) due to both the uncertainties in the Λ-core potential (error of about 5%, as mentioned above) and the no inclusion of the nuclear core distortion effects (errors of about of the same size than the statistical ones, as discussed in Subsects. 4.2 and 4.4). Adding all the systematic and statistical errors in quadratures we end up with total errors of about 7% for both the π^0 and π^- decay widths.

The main ($\geq 95\%$) contribution to these decay widths comes from processes where the outgoing nucleon is in a bound state of the daughter hypernucleus, processes described in Eqs. (37) – (38).

Note that the final nuclear state is described by means of a simple shell–model supplemented by an effective interaction (Cohen-Kurath) for the $1p-$shell nucleons. Results presented above might depend on the specific details of the used central and residual interactions. This is a problem, which is not specific of the mesonic decay of double$-\Lambda$ hypernuclei and it is already present in the studies of the mesonic decay of single $\Lambda-$hypernuclei. Indeed, if the residual interaction is neglected, we obtain with the potential of Eq. (47) values for decay widths (in units of Γ_Λ) of $0.074 \pm 0.004 \pm 0.004$ and $0.370 \pm 0.008 \pm 0.008$ for π^0 and π^- decays. The difference between these values and those quoted in Eqs. (66) – (67) might give us an estimate of the size of our uncertainties. A recent calculation of the π^- decay [40], where the nuclear states are been constructed in the shell model within $p-$shell configurations with Cohen-Kurath interaction [67], gives 0.325. This value fits within our range of results.

To minimize the effects of this new source of systematic errors, it is interesting to define the ratios

$$\frac{\Gamma({}^{13}_{\Lambda\Lambda}\mathrm{B} \rightarrow X + \Lambda + \pi^0)}{2\Gamma({}^{12}_{\Lambda}\mathrm{B} \rightarrow X + \pi^0)} = 0.63 \pm 0.02 \pm 0.02 \pm 0.02, \quad (68)$$

$$\frac{\Gamma({}^{13}_{\Lambda\Lambda}\mathrm{B} \rightarrow X + \Lambda + \pi^-)}{2\Gamma({}^{12}_{\Lambda}\mathrm{B} \rightarrow X + \pi^-)} = 0.67 \pm 0.02 \pm 0.02 \pm 0.02, \quad (69)$$

which differ from the naively expected value 1. These values have been obtained by using the potential of Eq. (47) and Cohen-Kurath $1p-$shell spectroscopic factors to describe the nuclear cores involved. Neglecting the residual interaction the potential of Eq. (47) leads to similar values (0.65 and 0.72 for π^0 and π^- decays respectively) for these ratios, as we expected. The meaning of the first two set of errors in the equations above is the same as in Eqs. (66) – (67). The last set of error accounts for the systematics due to the no inclusion of the nuclear core distortion effects. On the other hand, in these ratios, the uncertainties due to the details of the Λ-core potential mostly cancel out.

The mesonic decay depends both on the momentum carried by the outgoing nucleon (the greater the nucleon momentum, the less effective the Pauli suppression is) and on the tail of the overlap function defined in Eq. (51). The first factor is totally determined by the energy balance in the reaction, which is the same for all potentials used. Thus, the fact that the mesonic widths calculated in the VAR scheme do not depend appreciably on the specific potential means that all overlap functions have a similar behavior at large distances. This is shown for two potentials in the bottom plot of Fig. 6.

On the other hand, HF wave functions lead to results similar, within a 5%, to those presented in Eqs. (66) – (69) and one would again expect that both HF and VAR overlap functions have similar tails. This can be seen in the top plot of Fig. 6. Finally, in this figure we also compare the HF and VAR overlap functions with the Λ wave function in the daughter hypernucleus (φ_Λ). Because the ratio $B_{\Lambda\Lambda}/2B_\Lambda$ is greater than one, the exponential decay at large distances of φ_Λ is less pronounced. This, together with the change in the energy balance of the reaction, which makes more effective the Pauli blocking for double- than for single–Λ hypernuclei, explains why the ratios defined in Eqs (68) – (69) are smaller than one.

To finish this section, in Fig. 7 we show the A dependence of the ratios $\Delta B_{\Lambda\Lambda}/2B_\Lambda$ and $\Gamma({}^{A+2}_{\Lambda\Lambda}\mathrm{Z} \rightarrow X + \Lambda + \pi^{0,-})/2\Gamma({}^{A+1}_{\Lambda}\mathrm{Z} \rightarrow X + \pi^{0,-})$. As can be seen in the figure, we are able to give accurate predictions for both ratios which also turn out to be rather independent of the details, $g_{\omega\Lambda\Lambda}$ and $\Lambda_{\sigma\Lambda\Lambda}$, of the effective $\Lambda\Lambda$ interaction.

In Ref. [38] the A-dependece of $\Delta B_{\Lambda\Lambda}$ has been also studied within a Skyrme-Hartree-Fock approach. There, it is also found that $\Delta B_{\Lambda\Lambda}$ is a decreasing function of A. We find values for $\Delta B_{\Lambda\Lambda}$ within the broad range of possible results quoted in that reference.

4.7 Nuclear Medium and Free Space $\Lambda\Lambda$ Interactions.

It is essential to state that the $\Lambda\Lambda$ potentials determined in this work, effectively describe the dynamics of the $\Lambda\Lambda$ pair in the nuclear medium, but they do not describe

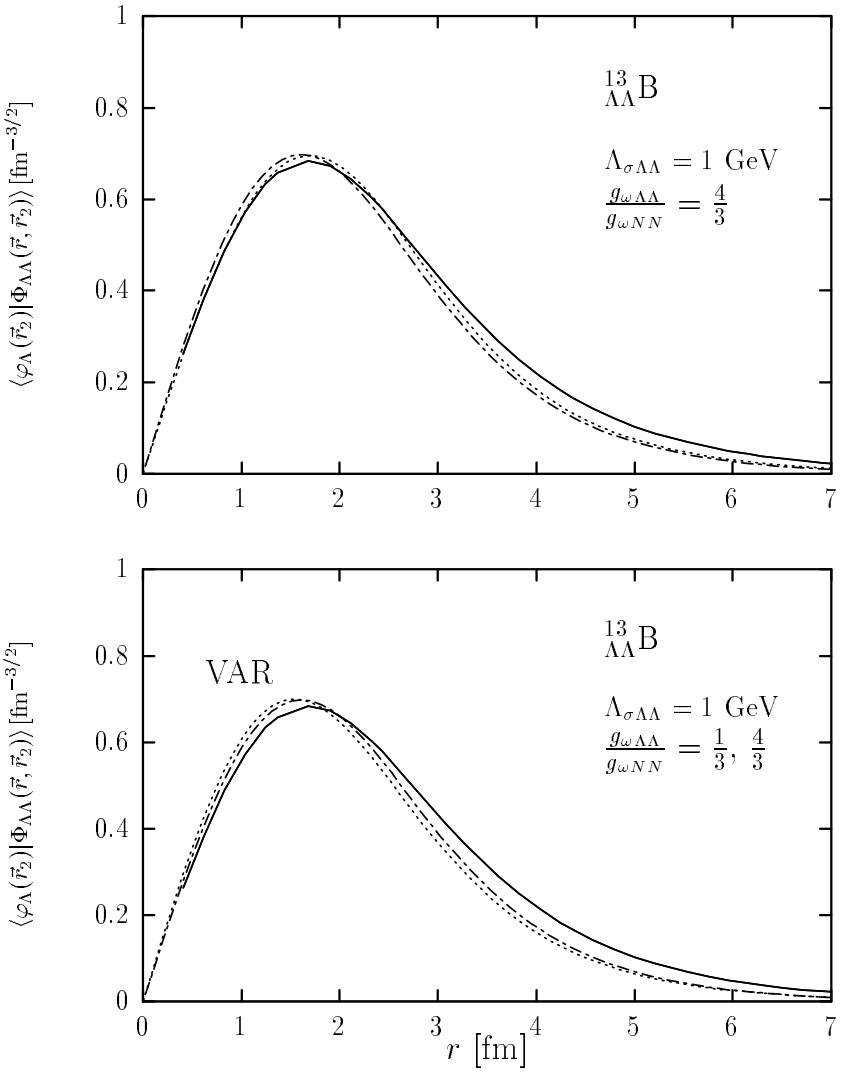

Figure 6: The projection of the two-particle $\Lambda\Lambda$ state in a double$-\Lambda$ hypernucleus, $\Phi_{\Lambda\Lambda}$, over the one-particle Λ state, φ_Λ, in the corresponding single–Λ hypernucleus is shown versus r for Boron. This projection is the overlap defined in Eq. (51). In all cases, the Λ-core interaction is of the BOY type and the cutoff parameter $\Lambda_{\sigma\Lambda\Lambda}$ is 1 GeV. The different lines correspond to different calculations of $\Phi_{\Lambda\Lambda}$ as follows. Top: Perturbative (solid), non-local HF (dotted) and VAR (dot-dashed) results, with $g_{\omega\Lambda\Lambda}/g_{\omega NN} = 4/3$ for the two last ones. Bottom: Perturbative (solid) and non-local VAR with two values for the ratio $g_{\omega\Lambda\Lambda}/g_{\omega NN}$, 1/3 (dotted) and 4/3 (dot-dashed). In the VAR and HF approaches $g_{\sigma\Lambda\Lambda}$ is obtained from the overall fit to the $B_{\Lambda\Lambda}$ data. Within the perturbative scheme, the overlap $\langle\varphi_\Lambda(\vec{r}_2)|\Phi_{\Lambda\Lambda}(\vec{r},\vec{r}_2)\rangle$ coincides with $\varphi_\Lambda(\vec{r})$ (Λ wave function in the $({}^{A+1}_{\Lambda}Z)$ hypernucleus).

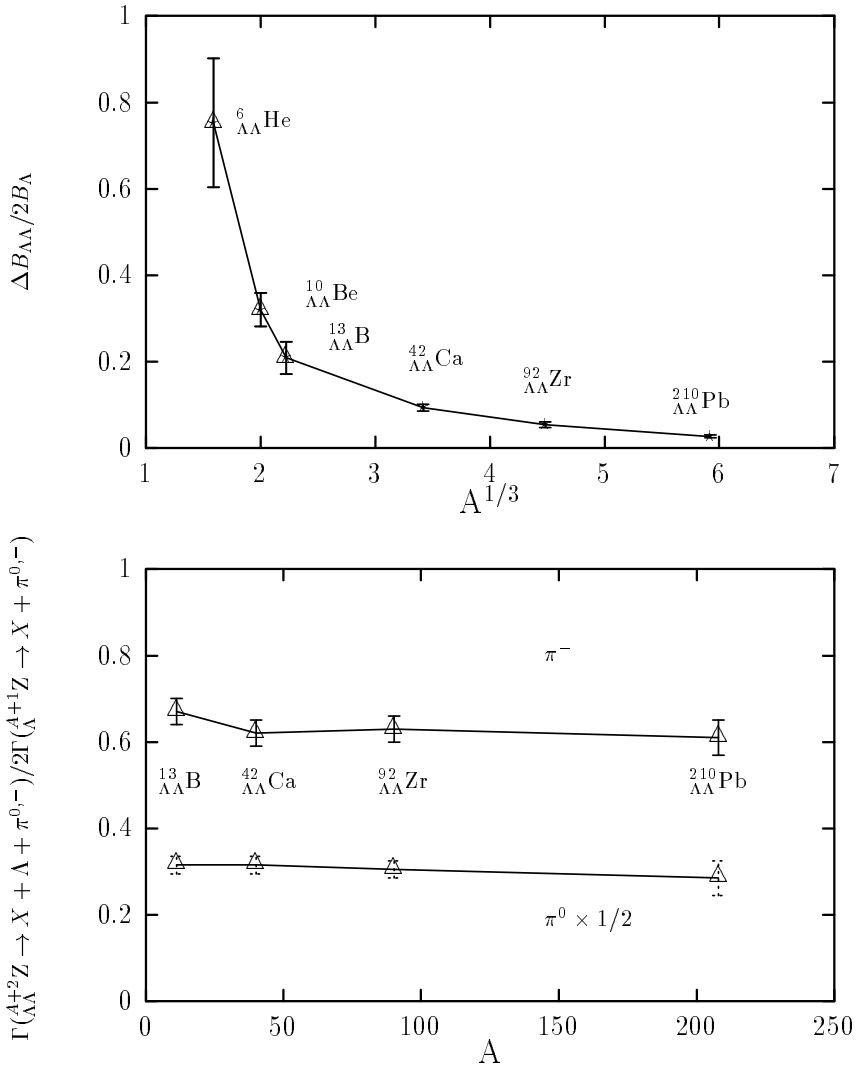

Figure 7: Ratios $\Delta B_{\Lambda\Lambda}/2B_\Lambda$ (top) and $\Gamma(^{A+2}_{\Lambda\Lambda}\mathrm{Z} \to X+\Lambda+\pi^{0,-})/2\Gamma(^{A+1}_{\Lambda}\mathrm{Z} \to X+\pi^{0,-})$ (bottom) computed for different double$-\Lambda$ hypernuclei. In the case of the ratio of mesonic widths with a π^0 in the final state, the results have been multiplied by a factor 1/2. BOY Λ-core potentials have been used for all hypernuclei and the non-local $\Lambda\Lambda$ interaction associated to $g_{\omega\Lambda\Lambda} = 2g_{\omega NN}/3$ and $\Lambda_{\sigma\Lambda\Lambda} = 1$ GeV has been used to determine the central value (see Table 8). Statistical and systematic errors in the fitted parameter $g_{\sigma\Lambda\Lambda}$ lead to the error bars in the shown ratios, as it is explained in the text after Eqs. (66) - (67). Experimental errors in B_Λ have not been considered. In some cases the size of the errors (systematic and statistical errors are added in quadrature) is smaller than the symbols.

their dynamics in the free space. Indeed, what has been determined in this work is an effective interaction in the medium. This effective interaction is usually approximated by an induced interaction [57, 75, 76] ($V^{ind}_{\Lambda\Lambda}$) which is built up in terms of the $\Lambda\Lambda \to \Lambda\Lambda$ ($G_{\Lambda\Lambda}$), $\Lambda N \to \Lambda N$ ($G_{\Lambda N}$) and $NN \to NN$ (G_{NN}) $G-$matrices, as depicted in Fig. 8. The induced interaction, $V^{ind}_{\Lambda\Lambda}$, has the virtue of combining the dynamics at short distances (accounted by the effective interaction $G_{\Lambda\Lambda}$) and at long distances (polarization phenomenon) which is taken care of by means of the iteration of the particle-hole (ph) excitations (RPA series) through the effective interactions $G_{\Lambda N}$ and G_{NN}. The $G_{\Lambda\Lambda}-$, $G_{\Lambda N}-$ and the $G_{NN}-$matrices can be obtained from the $S=-2$, $S=-1$ and $S=0$ baryon-baryon interactions in the free space [17, 24, 75]. In the $S=-2$ channel and near threshold, as discussed in the introduction, one needs to solve the $\Lambda\Lambda - \Xi N$ coupled channel G–matrix equations[16]. In a nuclear medium and with total energies of the order of $2m_\Lambda$, the $\Lambda\Lambda - \Xi N$ coupling might be suppresed due to Pauli blocking and thus the data of double$-\Lambda$ hypernuclei would probe primarily the $\Lambda\Lambda$ diagonal element[17], $V^{free}_{\Lambda\Lambda}$, of the $\Lambda\Lambda - \Xi N$ potential. Thus, $G_{\Lambda\Lambda}$ might be roughly approximated by $V^{free}_{\Lambda\Lambda}$.

To establish the connection between $V^{ind}_{\Lambda\Lambda}$ and $V^{free}_{\Lambda\Lambda}$ is the aim of a future work [55] and it is out of the scope of this work. As discussed above, it requires to understand the renormalization of the σ, ω propagation (it will be necessary to take into account that both carriers can excite ph components on their propagation through the nucleus [57, 68]) and the role played by the ΞN intermediate states in the nuclear medium. Note that, within the Bonn-Jülich model, the $\phi-$ meson does not couple to nucleons, and hence its propagation in the nuclear medium is not renormalized.

In Table 13 we present the smallest values of the $g_{\sigma\Lambda\Lambda}$ parameter which lead to $^1S_0$ $\Lambda\Lambda$ bound states in the free space, when $\sigma+\omega+\phi-$ $\Lambda\Lambda$ interactions, with different cutoffs for the ϕ potential, are considered. For the sake of simplicity, we have fixed $g_{\omega\Lambda\Lambda}/g_{\omega NN} = \frac{2}{3}$ and $\Lambda_{\sigma\Lambda\Lambda} = 1$ GeV. $\phi-$couplings are given in Eq. (65). As can be deduced from the numbers quoted in this table and those already presented in Table 11 the derived HF $\Lambda\Lambda$ potentials would lead to $\Lambda\Lambda$ bound states. However within the variational scheme in all cases the potentials are not attractive enough to bind the two hyperons[18].

Preliminary results of Ref. [55] show that the $\Lambda\Lambda$ interaction in the medium, $V^{ind}_{\Lambda\Lambda}$, is more attractive than that in the free space, $V^{free}_{\Lambda\Lambda}$. Variational results (our best results) provide effective interactions unable to bind the $\Lambda\Lambda$ pair in the $^1S_0$ channel. Therefore we can discard the existence of $\Lambda\Lambda$ bound states in the free space when only the $\Lambda\Lambda$ diagonal element, $V^{free}_{\Lambda\Lambda}$, of the $\Lambda\Lambda - \Xi N$ potential is considered. An independent confirmation of the no existence of $\Lambda\Lambda$ bound states is given by the $\sigma-$coupling ($g_{\sigma\Lambda\Lambda}/\sqrt{4\pi} = 2.138$) extracted from the study of hyperon-nucleon scattering processes which is well below of any of the $\sigma-$couplings quoted in Table 13. However, the $\Lambda\Lambda-\Xi N$ coupling, though likely

[16]The $\Lambda\Lambda - \Xi N$ mass difference is about 25 MeV. The mass difference between the $\Lambda\Lambda$ and $\Sigma\Sigma$ pairs is about 150 MeV. Thus one can safely neglect the influence of the latter channel in the study of the $\Lambda\Lambda$ dynamics at threshold.

[17]It is to say that the contribution of the $\Lambda\Lambda \to \Xi N \to \Lambda\Lambda$ transition would be much smaller than the direct $\Lambda\Lambda \to \Lambda\Lambda$ one (with no ΞN intermediate states and accounted for by the $V^{free}_{\Lambda\Lambda}$ piece of the $S=-2$ potential), in this context.

[18]The conclusion is the same for the case $\Lambda_{\sigma\Lambda\Lambda} = 2$ GeV.

	without ϕ	with ϕ		
$\Lambda_{\phi\Lambda\Lambda}$[GeV]	–	1.5	2.0	2.5
$g_{\sigma\Lambda\Lambda}/\sqrt{4\pi}$	3.098	3.105	3.003	2.889

Table 13: Smallest values of the $g_{\sigma\Lambda\Lambda}-$coupling leading to $^1S_0$ $\Lambda\Lambda$ bound states in the vacuum. Different non-local interactions, all of them with $g_{\omega\Lambda\Lambda}/g_{\omega NN} = \frac{2}{3}$ and $\Lambda_{\sigma\Lambda\Lambda} = 1$ GeV, without and with the inclusion of the $\phi-$meson exchange potential, which coupling to the hyperons is fixed by means of the $SU(6)-$symmetry, have been considered. In the latter case three different cutoffs have been studied.

suppresed in the nuclear medium, might contribute significantly in the free space. In the model proposed in Ref. [37], the inclusion of the above coupling leads to more attractive interactions in the $S = -2$ sector, allowing for values of the $\Lambda\Lambda$ $^1S_0$ free space scattering length as large as that of the nn system. Thus, to draw any firm conclusion about the existence of bound states in the $S = -2$ baryon-baryon sector, a combined studied of the $\Lambda\Lambda$ and ΞN systems is needed.

We would like to stress that the important issue now is to clarify whether or not the difference between the $g_{\sigma\Lambda\Lambda}/\sqrt{4}\pi$ values of 2.138 (obtained from hyperon-nucleon scattering data in Ref. [46]) and of 2.85 (obtained in this work for $g_{\omega\Lambda\Lambda}/g_{\omega NN} = 2/3$ and $\Lambda_{\sigma\Lambda\Lambda} = 1$ GeV within the VAR scheme[19]) can be explained in terms of medium renormalization effects and/or the contribution of ΞN intermediate states to the induced interaction $V^{ind}_{\Lambda\Lambda}$ and/or the contribution of heavier mesons not included here, such as the ϕ meson. As discussed in Subsect. 4.5, the inclusion of the $\phi-$exchange piece of the $\Lambda\Lambda$ potential reduces in some extent the difference between the $g_{\sigma\Lambda\Lambda}$ couplings mentioned above. For instance, if a $\Lambda_{\phi\Lambda\Lambda}$ cutoff of 2.5 GeV is used, one finds values for $g_{\sigma\Lambda\Lambda}/\sqrt{4}\pi$ of the order of 2.6 (Table 11).

Finally a word of caution must be said here. The Jülich group has also shown [77, 78] that the correlated 2π and $K\bar{K}$ exchanges lead to a value for the ratio $g_{\sigma\Lambda\Lambda}/g_{\sigma NN}$ of 0.49. This value is much smaller than the results obtained in any of the present YN models [43, 44, 45, 46, 47, 48], for which this ratio varies from 0.58 to 1. Therefore, the intermediate range attraction in the ΛN and $\Lambda\Lambda$ channels will be significantly reduced if one assumes the results of the microscopical calculations of Refs. [77, 78]. Then, a value for the ratio $g_{\omega\Lambda\Lambda}/g_{\omega NN}$ smaller than 2/3, predicted by $SU(3)$ and commonly accepted, would be needed to reproduce the ΛN scattering data. Thus, once all nuclear medium effects are understood, it will also be worth studying if a new set of parameters with $g_{\sigma\Lambda\Lambda}/g_{\sigma NN} = 0.49$ and $g_{\omega\Lambda\Lambda}/g_{\omega NN} < 2/3$ provides a simultaneous acceptable description of both double$-\Lambda$ hypernuclei and Λp scattering data.

[19]These values for the ratio $g_{\omega\Lambda\Lambda}/g_{\omega NN}$ and cutoff $\Lambda_{\sigma\Lambda\Lambda}$ correspond to those used in Ref. [46].

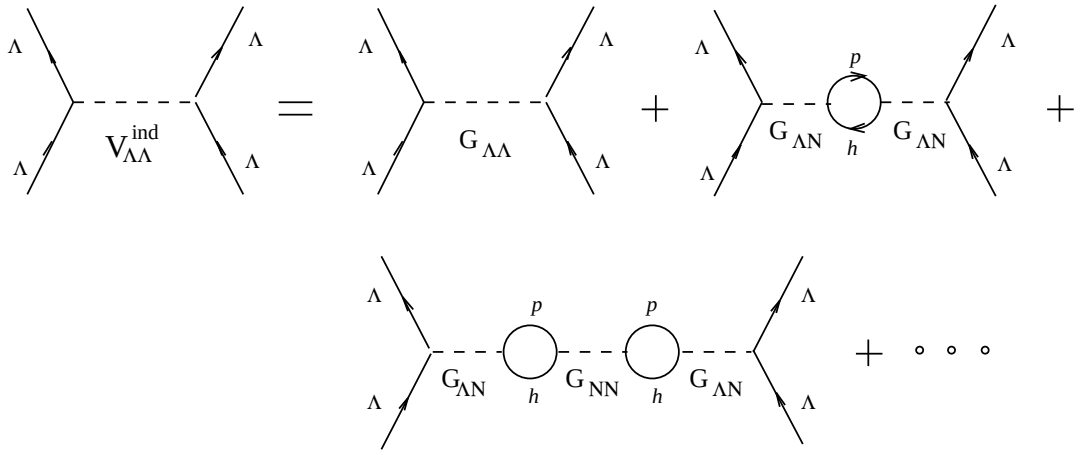

Figure 8: Feynman diagrams relating the $\Lambda\Lambda \to \Lambda\Lambda, \Lambda N \to \Lambda N$ and $NN \to NN$ G–matrices to the induced interaction ($V^{ind}_{\Lambda\Lambda}$) in the nuclear medium, which approximately accounts for the effective interaction determined in this work.

5 Conclusions

The dynamics of the $\Lambda\Lambda$ system can not be studied directly in the free space. $\Lambda\, p$ scattering provides an indirect source of information about it. Thus, the physics of double$-\Lambda$ hypernuclei provides an independent and valuable method to confirm the findings obtained in the studies of hyperon-nucleon scattering. From these studies, it is commonly accepted that there exist three kinds of realistic models for the $\Lambda\Lambda$ diagonal element of the $\Lambda\Lambda - \Xi N$ potential, those developped by the Nijmegen, Tübingen and Jülich groups. The Jülich OBE potential for the hyperon-hyperon interaction is a natural extension of the Bonn model for the NN-interaction [49]. In this paper we have used for the first time Jülich type $\Lambda\Lambda$ OBE potentials to study the dynamics of double$-\Lambda$ hypernuclei. We have found:

- Effective $\Lambda\Lambda$ interactions in the medium extracted from Jülich type models provide a simultaneous fairly good description of the binding energies of the three known double$-\Lambda$ hypernuclei.

- Uncertainties in the exact nature of the Λ-nuclear core dynamics lead to uncertainties in the determination of the effective $\Lambda\Lambda$ potential in the medium smaller than those due to the experimental errors in the fitted quantities $\Delta B_{\Lambda\Lambda}$. Thus, the ambiguities in the determination of the Λ-core potential do not constitute an important obstacle to learn details about the $\Lambda\Lambda$ interaction.

- The HF and the perturbative approaches, discussed in Subsects. 4.2 and 4.3 respectivelly, lead to quite similar effective $\Lambda\Lambda$ potentials.

- The inclusion of $\Lambda\Lambda$ correlations in the variational scheme provides a better understanding of the dynamical features of the system. It also enables less attractive

effective $\Lambda\Lambda$ potentials than in the HF or perturbative approaches and more similar to those extracted from hyperon-nucleon scattering to describe the binding energies of the double$-\Lambda$ hypernuclei.

- Only few waves (up to $l = 3$) contribute appreciably to the multipolar expansion of the VAR wave functions.

- The inclusion of the $\phi-$exchange might be relevant to understand the effective $\Lambda\Lambda$ interaction derived in this work in terms of the free space one.

- The existing double$-\Lambda$ hypernuclei data can not conclusively favour any particular choice neither of the ratio $g_{\omega\Lambda\Lambda}/g_{\omega NN}$ in the interval $[1/3, 4/3]$ around the $SU(3)$ prediction $2/3$, nor of the cuttoff $\Lambda_{\sigma\Lambda\Lambda}$ in the range = 1–2 GeV. Thus, we end up with a whole family of effective $\Lambda\Lambda$ potentials describing the ground state binding energy of the three known double$-\Lambda$ hypernuclei.

- The mesonic decay of ${}^{13}_{\Lambda\Lambda}$B and the binding energies and pionic decay widths of heavier double$-\Lambda$ hypernuclei (not discovered yet) turned out to be rather independent of the details of the effective $\Lambda\Lambda$ interaction within the family of potentials described in the previous point. This fact has allowed us to predict accurately, for the very first time, the mesonic decay widths of medium and heavy double$-\Lambda$ hypernuclei.

- We have discarded the existence of ${}^1S_0$ $\Lambda\Lambda$ bound states in the free space if the $\Lambda\Lambda - \Xi N$ coupling is negligible.

The natural continuation of this work [55] is the study of the nuclear medium modifications of the $\Lambda\Lambda$ interaction. Such study, together with the effective $\Lambda\Lambda$ interactions derived here, will allow us to better understand the dynamical features of the $\Lambda\Lambda$ interaction, at low energies, in the vacuum. Thus, it will be possible to contrast features of such interaction from two different and independent sources of data: hyperon-nucleon scattering and $\Lambda\Lambda$ hypernuclei. Statisticaly improved and new experimental data on double$-\Lambda$ hypernuclei, exploring not only light but also medium and heavy nuclei, will be extremely valuable to achive such an objective.

Acknowledgments

We would like to acknowledge useful discussions with E. Buendía, F. Gálvez, A. Ramos, L.L. Salcedo and A. Sarsa. J.C. thanks the Departamento de Física Moderna in Granada for its kind hospitality during the early stages of this project. This research was supported by DGES under contract PB95-1204 and by the Junta de Andalucía. J.C. acknowledges the Spanish Dirección General de Enseñanza Superior (Ministry of Science and Education) for support through a postdoctoral fellowship.

Appendix
Matrix Elements in the VAR Scheme

The basic integrals to compute the matrix elements of the hamiltonian of Eq. (5) in the basis defined in Eq. (10) are:

$$\Gamma_{lmn}(a,c) \;=\; 8\pi^2 \int_0^{+\infty} dr_1\, r_1^l \int_0^{+\infty} dr_2\, r_2^m \int_{|r_1-r_2|}^{r_1+r_2} dr_{12}\, r_{12}^n\; e^{-(a(r_1+r_2)+c\,r_{12})}\,, \qquad (70)$$

with a, c and l, m, n real positive and integer numbers respectively. To compute the matrix elements of the Λ kinetic terms, of the HE term, of the Λ-core potentials and of the local part of the $\Lambda\Lambda$ interaction, only non-negative values of l, m and n are needed. In this case, all the integrals can be obtained from Γ_{000} by means of a recursion formula proposed in Ref. [65]:

$$\Gamma_{lmn} \;=\; \frac{1}{2a}\left[l\,\Gamma_{l-1,m,n} + m\,\Gamma_{l,m-1,n} + B_{lmn}\right], \qquad (71)$$

$$B_{lmn} \;=\; \frac{1}{a+c}\left[l\,B_{l-1,m,n} + n\,B_{l,m,n-1} + \delta_{l\,0}\frac{(4\pi)^2(m+n)!}{(a+c)^{m+n+1}}\right], \qquad (72)$$

with Γ_{000} given by:

$$\Gamma_{000} \;=\; \frac{(4\pi)^2}{2a(a+c)^2}\,. \qquad (73)$$

To compute the matrix elements of the non-local part of the $\Lambda\Lambda$ interaction, integrals of the type $\Gamma_{l,m,-1}$, with $l, m = 0, 1, 2\cdots$ are also needed. These can be obtained from a recursion as well [66],

$$\Gamma_{l,m,-1} \;=\; \frac{1}{2a}\left[l\,\Gamma_{l-1,m,-1} + m\,\Gamma_{l,m-1,-1} + \frac{l!\,m!}{l+m+1}\frac{(4\pi)^2}{(a+c)^{l+m+1}}\right], \qquad (74)$$

with $\Gamma_{0,0,-1}$ given by

$$\Gamma_{0,0,-1} \;=\; \frac{(4\pi)^2}{2a(a+c)}\,. \qquad (75)$$

A final detail, related to the non-local part of the $\Lambda\Lambda$ interaction, concerns to the implementation of $\vec{\nabla}_{12}$ when acting on functions of r_1,r_2 and r_{12}. The operator $\vec{\nabla}_{12}$ has to be understood as the gradient on the direction $\vec{r}_{12} = \vec{r}_1 - \vec{r}_2$ when the coordinates of the center of mass of the $\Lambda\Lambda$ pair, $\vec{R}_{cm} = (\vec{r}_1 + \vec{r}_2)/2$, are kept fixed. Thus,

$$\vec{\nabla}_{12} f(r_1, r_2, r_{12}) \;=\; \frac{1}{2}\left(\vec{\nabla}_1 - \vec{\nabla}_2\right) f(r_1, r_2, r_{12}), \qquad (76)$$

$$\;=\; \frac{1}{2}\left(\frac{\vec{r}_1}{r_1}\frac{\partial}{\partial r_1} - \frac{\vec{r}_2}{r_2}\frac{\partial}{\partial r_2} + 2\frac{\vec{r}_{12}}{r_{12}}\frac{\partial}{\partial r_{12}}\right) f(r_1, r_2, r_{12}), \qquad (77)$$

with $\vec{\nabla}_{1\,(2)}$ the gradient on the direction $\vec{r}_{1\,(2)}$ when $\vec{r}_{2\,(1)}$ is kept fixed.

References

[1] D.H. Davis, Nucl. Phys. **A547** (1992) 369c; D. H. Davis and J. Pniewsky, Contemp. Phys. **27** (1986) 91 and references therein.

[2] B. Bohm *et al.*, Nucl. Phys. **B4**, (1968) 511.

[3] P.H. Pile, *et al.*, Phys. Rev. Lett. **66** (1991) 2585.

[4] T. Hasegawa, *et al.*, Phys. Rev. **C53** (1996) 1210.

[5] D. J. Prowse, Phys. Rev. Lett. **17** (1966) 782.

[6] M. Danysz *et al.*, Nucl. Phys. **49** (1963) 121. Reanalysis of R.H. Dalitz *et al.*, Proc. R. Soc. London **A426** (1989) 1.

[7] S. Aoki *et al.*, Prog. Theor. Phys. **85** (1991) 1287.

[8] K. Imai, Nucl. Phys. **A547** (1992) 199c.

[9] K. Nakazawa, Nucl. Phys. **A585** (1995) 75c; *ibidem* Proc. of Intern. Conf. on Hypernuclear and Strange Particle Physics, Brookhaven 1997, Nucl. Phys. A in print, Eds. R. E. Chrien and D. J. Millener.

[10] G.B. Franklin, Nucl. Phys. **A585** (1995) 83c.

[11] M. May, Proc. of Intern. Conf. on Hypernuclear and Strange Particle Physics, Brookhaven 1997, Nucl. Phys. A in print, Eds. R. E. Chrien and D. J. Millener.

[12] R. Brockmann and W. Weise, Phys. Lett. **B69** (1977) 167.

[13] A. Bouyssy, Phys. Lett. **B84** (1979) 41.

[14] R. Brockmann and W. Weise, Nucl. Phys. **A355** (1981) 365.

[15] A. Bouyssy, Nucl. Phys. **A381** (1982) 445.

[16] A.R. Bodmer, Q.N. Usmani and J. Carlson, Nucl. Phys. **A422** (1984) 510.

[17] Y. Yamamoto and H. Bando, Prog. of Theor. Phys. **73** (1985) 905.

[18] A.R. Bodmer and Q.N. Usmani, Nucl. Phys. **A468** (1987) 653; *ibidem* Nucl. Phys. **A477** (1988) 621.

[19] D.J. Millener, C.B. Dover and A. Gal, Phys. Rev. **C38** (1988) 2700.

[20] K. Itonaga, T. Motoba and H. Bando, Z. Phys. **A330** (1988) 209.

[21] J. Mares and J. Zofka, Z. Phys. **A333** (1989) 209; *ibidem*, Z. Phys. **A345** (1993) 47.

[22] T. Motoba, H. Bando, T. Fukuda and J. Zofka, Nucl. Phys. **A534** (1991) 597; T. Motoba, Nucl. Phys. **A547** (1992) 115c.

[23] T. Motoba, Nucl. Phys. **A527** (1991) 485c; *ibidem* Nucl. Phys. **A547** (1992) 115c.

[24] Y. Yamamoto, H. Takaki and K. Ikeda, Prog. of Theor. Phys. **86** (1991) 867.

[25] C. B. Dover, D.J. Millener, A. Gal and D.H. Davis, Phys. Rev. **C44** (1991) 1905.

[26] Y. Akaishi, Nucl. Phys. **A547** (1992) 217c.

[27] Y. Yamamoto, Nucl. Phys. **A547** (1992) 233c; Y. Yamamoto, *et al.*, Prog. Theor. Phys. Suppl. No. **117** (1994) 361.

[28] H. Himeno, T. Sakuda, S. Nagata and Y. Yamamoto, Prog. Theor. Phys. **89** (1993) 109.

[29] U. Straub, J. Nieves, A. Faessler and E. Oset, Nucl. Phys. **A556** (1993) 531.

[30] J. Nieves and E. Oset, Phys. Rev. **C47** (1993) 1478.

[31] R. Guardiola and J. Navarro, Acta Phys. Pol. **B24** (1993) 525; *ibidem* Condes. Matter Theories **9** (1994) 367.

[32] D. Halderson, Phys. Rev. **C** 48 (1993) 581.

[33] J. Mares and K. Jennings, Phys. Rev. **C49** (1994) 2472.

[34] E. Oset, *et al.*, Prog. Theor. Phys. Suppl. No. **117** (1994) 461.

[35] J. Schaffner *et al*, Ann. Phys. (N.Y.) **235** (1994) 35.

[36] Z. Ma, *et al.*, Nucl. Phys. **A608** (1996) 305.

[37] S.B. Carr, I.R. Afnan and B.F. Gibson, Nucl. Phys. **A625** (1997) 143.

[38] D.E. Lanskoy, Y. A. Lurie and A. M. Shirokov, Z. Phys. **A357** (1997) 95.

[39] Y. Yamamoto, M. Wakai, T. Motoba and T. Fukuda, Nucl. Phys. **A625** (1997) 107.

[40] T. Motoba, Talk at "Workshop on The Weak Decay of Hypernuclei", ECT*, Trento, Italy, July 1998.

[41] E. Oset and A. Ramos, Prog. Part. Nucl. Phys., vol. **41**, (1998) 191.

[42] Proceedings of International Conferences on Hypernuclear and Strange Particle Physics: Nucl. Phys. **A547** (1992), Nucl. Phys. **A585** (1995), Nucl. Phys. **A639** (1998).

[43] P.M.M. Maessen, Th. A. Rijken and J.J. de Swart, Phys. Rev. **C40** (1989) 2226.

[44] M.M. Nagels, T.A. Rijken and J.J. de Swart, Phys. Rev **D12** (1975) 744; Phys. Rev **D15** (1977) 2547; Phys. Rev **D20** (1979) 1633.

[45] B. Holzenkamp, K. Holinde and J. Speth, Nucl. Phys. **A500** (1989) 485.

[46] A. Reuber, K. Holinde and J. Speth, Nucl. Phys. **A570** (1994) 543.

[47] U. Straub, *et al.*, Nucl. Phys. **A483** (1988) 686.

[48] U. Straub, *et al.*, Nucl. Phys. **A508** (1990) 385c.

[49] R. Machleidt, K. Holinde and Ch. Elster, Phys. Reports **149** (1987)1.

[50] A. R. Bodmer and S. Ali, Phys. Rev. **138** (1965) B465 ; *ibidem* Phys. Lett. **24B** (1967) 343.

[51] R. L. Jaffe, Phys. Rev. Lett. **38**, (1977) 195 ; *ibidem* **38**, (1977) 617(E).

[52] M. P. Locher, M. E. Sainio and A. Svarc, Advances in Nuclear Physics vol. **17** (1986) 47 Eds. J.W. Negele and E. Vogt.

[53] C.B. Dover and H. Feshbach, Ann. Phys. (N.Y.) **198** (1990) 321.

[54] C.B. Dover, Nucl. Phys. **A450** (1986) 95c.

[55] J. Caro, C. García-Recio and J. Nieves, in preparation.

[56] A. Galindo and P. Pascual, *Quantum Mechanics*, Springer, New York, 1991.

[57] A.L. Fetter and J.D. Walecka, *Quantum Theory on Many Particle Systems*, McGraw-Hill, New York, 1971.

[58] K. Frankowski and C.L. Pekeris, Phys. Rev. **146** (1966) 46.

[59] D. E. Freund, B. D. Huxtable and J.D. Morgan III, Phys. Rev **A29** (1984) 980.

[60] H. Kleindienst and R. Emrich, Int. Quantum Chemistry, **37** (1990) 257.

[61] F. Arias de Saavedra and E. Buendía, J. Phys. **B**: At. Mol. Opt. Phys. 27 (1994) 1277.

[62] E.A. Hylleraas, Z. Phys. **48** (1928) 469; *ibidem* , **54** (1929) 347.

[63] L. Pauling and E.B. Wilson, *Introduction to Quantum Mechanics*, McGraw-Hill, London, 1935.

[64] F. Arias de Saavedraa, E. Buendía, F.J. Gálvez and A. Sarsa, Eur. Phys. Jour. **D2** (1998) 181.

[65] R.A. Sack, C.C.J. Roothaan and W. Kolos, Jour. Math. Phys. **8** (1967), 1093.

[66] J. Caro, Phys. Rev. **A** in print, University of Müenchen preprint (1998), physics/9803003.

[67] S. Cohen and D. Kurath, Nucl. Phys. **73** (1965) 1.

[68] J. Nieves, E.Oset and C.García-Recio, Nucl. Phys. **A554** (1993) 509.

[69] J. Nieves, E.Oset and C.García-Recio, Nucl. Phys. **A554** (1993) 554.

[70] P.E.Hodgson, *Nuclear Reactions and Nuclear Structure*, Oxford University Press, England, 1971.

[71] S. Cohen and D. Kurath, Nucl. Phys. **A101** (1967)1.

[72] M.H. Macfarlane and J.B. French, Rev. Mod. Phys. **32** (1960) 567.

[73] P.J. Brussaard and P.W.M. Glaudemans, *Shell Model Applications in Nuclear Spectroscpy*, North Holland, 1971.

[74] C.W. de Jager, H. de Vries and C. de Vries, Atomic Data and Nuclear Data Tables **14** (1974) 479.

[75] G.E. Brown, *Many-Body Problems* , North Holland Amsterdam 1972.

[76] E. Oset, P. Fernández de Córdoba, L.L. Salcedo and R. Brockman, Phys. Rep. **188** (1990) 79.

[77] K. Holinde, H.C. Kim, A. Reuber and J. Speth, Nucl. Phys. **A585** (1995) 149c.

[78] A. Reuber, K. Holinde, H.C. Kim and J. Speth, Nucl. Phys. **A608** (1996) 243.